A Comprehensive Theoretical Study on the Reactions of Sc^+ with C_nH_{2n+2} ($n = 1-3$): Structure, Mechanism, and Potential-Energy Surface

Dongju Zhang,*[b] Chengbu Liu,*[a] Siwei Bi,[a] and Shiling Yuan[b]

Abstract: The reactions of $Sc^+(^3D)$ with methane, ethane, and propane in the gas phase were studied theoretically by density functional theory. The potential energy surfaces corresponding to [Sc, C_n, H_{2n+2}]$^+$ ($n = 1-3$) were examined in detail at the B3LYP/6-311++G(3df, 3pd)//B3LYP/6-311+G(d,p) level of theory. The performance of this theoretical method was calibrated with respect to the available thermochemical data. Calculations indicated that the reactions of Sc^+ with alkanes are multichannel processes which involve two general mechanisms: an addition–elimination mechanism, which is in good agreement with the general mechanism proposed from earlier experiments, and a concerted mechanism, which is presented for the first time in this work. The addition–elimination reactions are favorable at low energy, and the concerted reactions could be alternative pathways at high energy. In most cases, the energetic bottleneck in the addition–elimination mechanism is the initial C–C or C–H activation. The loss of CH_4 and/or C_2H_6 from $Sc^+ + C_nH_{2n+2}$ ($n = 2$, 3) can proceed along both the initial C–C activation branch and the C–H activation branch. The loss of H_2 from $Sc^+ + C_nH_{2n+2}$ ($n = 2$, 3) can proceed not only by 1,2-H_2 and/or 1,3-H_2 elimination, but also by 1,1-H_2 elimination. The reactivity of Sc^+ with alkanes is compared with those reported earlier for the reactions of the late first-row transition-metal ions with alkanes.

Keywords: alkanes · C–C activation · C–H activation · density functional calculations · scandium

Introduction

C–H and C–C activations of hydrocarbons at metal centers are of fundamental importance in various areas of chemistry, such as biochemistry, organometallic chemistry, and homo- and heterogeneous catalysis.[1–2] The reactions of first-row transition-metal ions with simple alkanes in the gas phase have been studied by many experimental techniques (e.g., ion-beam mass spectrometry, ion cyclotron resonance mass spectrometry, high-pressure mass spectrometry, flowing afterglow methods, and collisional activation by tandem mass spectrometry)[1–9] following the observation by Allison et al.[10] that atomic transition-metal ions can activate C–C and C–H bonds in alkanes. These experiments provided valuable insights into reactions between transition-metal ions and hydrocarbons, and substantial quantitative thermochemical data is now available for a number of such systems. In recent years considerable efforts have been directed at understanding the mechanism and energetics of C–H and C–C bond activation by transition-metal ions.

In the reactions of transition-metal ions with CH_4, C_2H_6, and C_3H_8, the products of Equations (1)–(19) are observed in general.

$$M^+ + CH_4 \rightarrow MH^+ + CH_3 \quad (1)$$

$$M^+ + CH_4 \rightarrow MCH_3^+ + H \quad (2)$$

$$M^+ + CH_4 \rightarrow MCH_2^+ + H_2 \quad (3)$$

$$M^+ + C_2H_6 \rightarrow M(C_2H_4)^+ + H_2 \quad (4)$$

$$M^+ + C_2H_6 \rightarrow MCH_2^+ + CH_4 \quad (5)$$

$$M^+ + C_2H_6 \rightarrow MCH_3^+ + CH_3 \quad (6)$$

$$M^+ + C_2H_6 \rightarrow MC_2H_2^+ + 2H_2 \quad (7)$$

$$M^+ + C_2H_6 \rightarrow MH_2^+ + C_2H_4 \quad (8)$$

$$M^+ + C_2H_6 \rightarrow MH^+ + C_2H_5 \quad (9)$$

$$M^+ + C_3H_8 \rightarrow MH^+ + C_3H_7 \quad (10)$$

$$M^+ + C_3H_8 \rightarrow MC_3H_7^+ + H \quad (11)$$

$$M^+ + C_3H_8 \rightarrow MCH_3^+ + C_2H_5 \quad (12)$$

$$M^+ + C_3H_8 \rightarrow MC_2H_5^+ + CH_3 \quad (13)$$

[a] Prof. Dr. C. Liu, S. Bi
Institute of Theoretical Chemistry, Shandong University
Jinan, 250100 (P. R. China)
E-mail: cbliu@sdu.edu.cn

[b] Dr. D. Zhang, S. Yuan
College of Chemistry and Chemical Engineering
Shandong University, Jinan, 250100 (P. R. China)
Fax: (+86) 531-8564464
E-mail: zhangdj@sdu.edu.cn

0947-6539/03/0902-0484 $ 20.00+.50/0 *Chem. Eur. J.* **2003**, *9*, No. 2

$$M^+ + C_3H_8 \rightarrow MC_3H_6^+ + H_2 \quad (14)$$

$$M^+ + C_3H_8 \rightarrow MH_2^+ + C_3H_6 \quad (15)$$

$$M^+ + C_3H_8 \rightarrow MC_2H_4^+ + CH_4 \quad (16)$$

$$M^+ + C_3H_8 \rightarrow MCH_4^+ + C_2H_4 \quad (17)$$

$$M^+ + C_3H_8 \rightarrow MCH_2^+ + C_2H_6 \quad (18)$$

$$M^+ + C_3H_8 \rightarrow MC_2H_6^+ + CH_2 \quad (19)$$

Here, M^+ denotes a transition-metal ion. For a given metal ion only some of these reactions may be involved under certain conditions. These reactions have generally been understood in terms of the mechanisms shown in Scheme 1.

For reactions $M^+ + CH_4$, the energetically most favorable process observed by experiment is dehydrogenation to form $MCH_2^+ + H_2$ at low energy. The proposed two main mechanisms for the process are shown in Scheme 1 (top). One involves a four-centered transition state (TS), and the other a dihydrido species. In reactions of M^+ with C_2H_6 and C_3H_8, the oxidative addition of C–H and C–C bonds to the metal center are two fundamental steps from which a series of products results, such as small neutral molecules (H_2, CH_4, C_2H_4, etc.) and fragmentation ions. Most of the mechanisms proposed in Scheme 1 (middle and bottom) involve a β-H or β-CH_3 shift after insertion of the metal ions into a C–C or C–H bond.

Although experimental techniques can provide general mechanisms for the reactions of transition-metal ions with small alkanes, as shown in Scheme 1, complete information on all elementary reactions involved in such reactions is only attainable in a few cases. The rational explanations of these observations requires the support of accurate potential energy surfaces (PES), and hence further theoretical studies are needed. Extensive theoretical studies on these reactions can not only evaluate experimental suggestions, but can also give new findings that could not be achieved experimentally under the considered conditions. Apparently, much more effort has been devoted to experimental research than to theoretical studies on these reactions, especially the detailed examination of the PES. Recently, several theoretical studies on the reactions of late first-row transition-metal ions with small alkanes such as CH_4, C_2H_6, and C_3H_8 were reported.[11–15] Although the reaction mechanism of Sc^+ with CH_4 was also reported by Musaev et al.,[16] comprehensive theoretical studies on the reactions of early first-row transition-metal ions with small alkanes are still necessary, since the electronic configurations of early transition-metal ions and the strength of spin–orbit interactions clearly differ from those of late first-row transition-metal ions. Most of the d orbitals are occupied in late transition-metal ions, while some of them are empty in early transition-metal ions. Hence distinct differences in the reactivities of early and late transition-metal ions can be expected. These reactions deserve more detailed theoretical studies. We chose Sc^+, which has only two valence electrons and is the simplest transition-metal ion, as a representative early first-row transition-metal ion. Here we describe in detail the interesting properties of the PESs of $[Sc, C_n, H_{2n+2}]^+$ ($n = 1-3$) and how the scandium ion activates C–H and C–C bonds in small alkanes. We expect to thus obtain a general profile of the elementary mechanisms of early first-row tran-

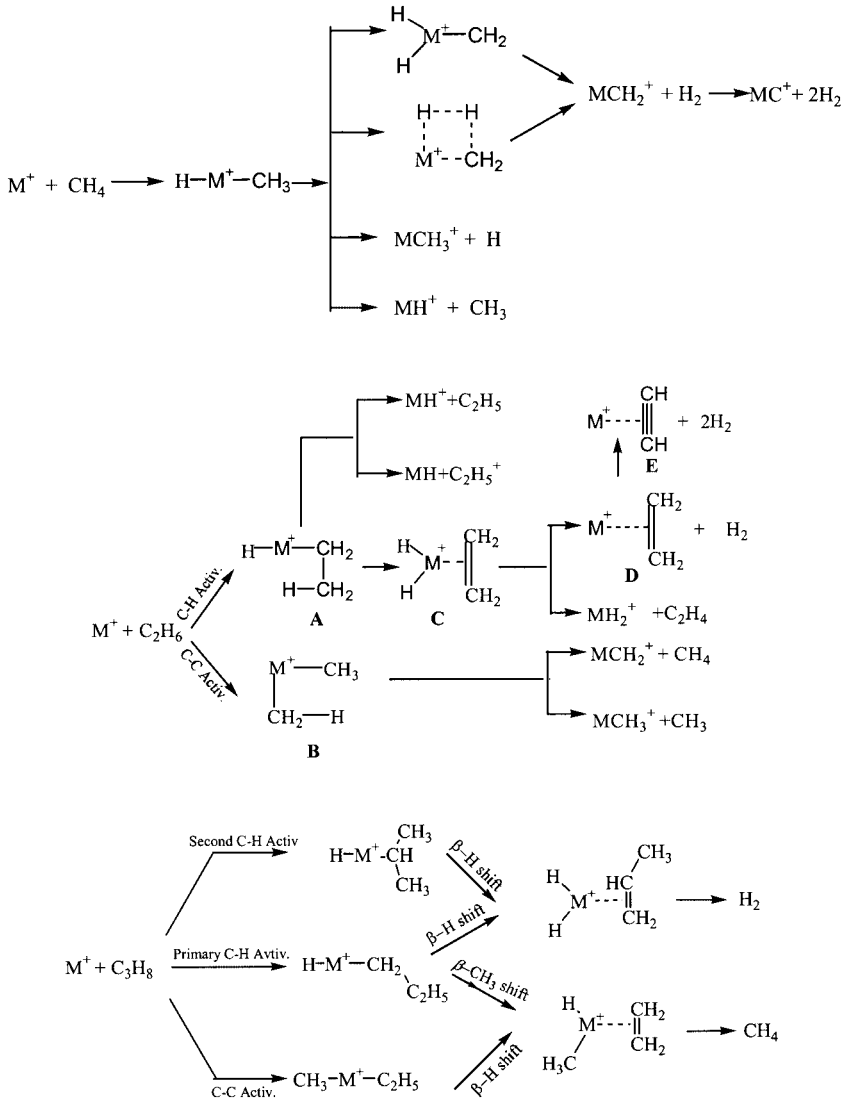

Scheme 1. General mechanisms for the reactions of transition-metal ions with methane (top) and ethane (middle), and for the CH_4 and H_2 eliminations of transition-metal ions with propane (bottom).

  0947-6539/03/0902-0485 $ 20.00+.50/0

sition-metal ions with small alkane by studying prototypes, and to reveal the differences in reactivities between early and late first-row transition-metal ions.

Quantum chemical ab initio calculations can in principle provide reliable information on molecular geometries and system energies. However, their computational complexity usually prevents their application to large molecules. Performing accurate calculations on systems involving transition metals by ab initio molecular orbital theory is difficult, since a relatively large number of electrons is present. As an alternative, density functional theory (DFT)[17, 18] has recently been widely applied to electronic structure calculations on systems that contain transition metals. The electron correlation effect in these systems is expected to play an important role in determining the system energetics and electronic configurations. The DFT method is particularly useful and computationally efficient for systems with a relatively large number of electrons that are difficult to deal with in ab initio molecular orbital theory.[19, 20] Furthermore, the spin contamination in the Kohn–Sham single determinant reference function proved to be relatively small. In view of the computational effectiveness and reliability of DFT, it was utilized throughout this work.

Methods of Calculation

We chose the B3LYP[21–24] DFT functional. This hybrid functional includes three fitted parameters and a mixture of Hartree–Fock exchange and DFT exchange correlation. This model provides reasonably accurate geometries and relative energies for organometallic systems,[25–27] and its reliability is generally comparable to that of the MP2 method.[28–31] Furthermore it requires far less disk space and is fast enough to allow the calculations performed in this study. In addition, previous studies have shown that B3LYP is highly suitable for ion–ligand complexes.[32–34] This functional has been widely used recently, especially for systems involving transition metals.

In special calculations, the full geometry optimizations on all the species involved in the reactions of scandium ion with C_nH_{2n+2} ($n=1-3$) were first performed at the B3LYP/6-311+G(d,p) level of theory without any imposed symmetry constraints. The standard 6-311+G(d,p) basis set is flexible enough to give a good account of longer range ion–ligand interactions. In addition, this basis set is large enough to generally reduce the basis set superposition error to less than the errors inherent in the method, so that superposition error corrections become unnecessary.

All stationary points were positively identified as minima or first-order saddle points by evaluation of the frequencies and normal modes. Further, several pathways between the transition structures and their corresponding minima were characterized by internal reaction coordinate (IRC)[35] calculations.

To analyze the sensitivity of the potential-energy surface to basis set and correlation effects, the relative energies were also reevaluated by using the large 6-311++G(3df,3pd) basis set. In all single-point energy calculations, the SCF convergence criterion was set to 10^{-8} to give a good energy convergence, since the basis sets used in this work include diffuse functions. For all cited energies, zero-point energy corrections have been included.

Since the accuracy of DFT calculations also depends on the number of points used in the numerical integration in addition to the sources of numerical errors in Hartree–Fock calculations, fine grids should be employed. In the present calculations, we used the default grid, which is a pruned (75,302) grid which has 75 radical shell and 302 angular points per shell and results in about 7000 points per atom. All processes described here occur on both the relevant triplet and singlet PESs. All calculations were performed with the Gaussian 98 program package[36] on an SGI 2100 server.

Results and Discussion

To check the reliability of our calculations, we first calibrated the calculated data against available experimental values to determine the performance of the level of theory. Then we examined reactions of Sc^+ with C_nH_{2n+2} ($n=1-3$) in detail, including the geometries of the various species involved in these reactions, the multichannel reaction mechanisms, the PES profiles, and comparison of the reactivity of Sc^+ with small alkanes to those of late first-row transition-metal ions.

Calibration of theoretical calculations: To clarify the general reliability of the theoretical calculations, we compared the predicted chemical properties of the present systems with corresponding experimental data.

Ionization potential of scandium: The scandium ion has a ^3D, 3d4s ground state, and the first ionization potential (IP) of scandium is 6.56 eV.[37] The calculated IPs of Sc at the B3LYP/6-311+G(d,p) and B3LYP/6-311++G(3df, 3pd) levels are 6.57 and 6.58 eV, respectively. The results obtained with both basis sets are in excellent agreement with the experimental value.

Bond dissociation energies: Accurate thermochemical data are available in the literature for the species involved in the reactions of transition-metal ions with small alkanes. Table 1 compares calculated bond dissociation energies (BDE) of several species involved in the considered reactions at the B3LYP/6-311+G(d,p) and B3LYP/6-311++G(3df,3pd) levels with corresponding experimental values. To allow for a more direct comparison to the experiment, the theoretical BDEs were corrected to 0 K by including zero-point vibrational energy. Use of the larger basis set apparently does not improve the DBE, and this confirms that the 6-311+G(d,p) basis set is flexible enough to describe the electronic characters of the species involved in the reactions of Sc^+ with C_nH_{2n+2} ($n=1-3$). The results obtained with the two basis sets are in good agreement, and this gives us confidence that the B3LYP/6-311+G(d,p) level is adequate to optimize the geometries and calculate the frequencies.

Table 1. Calculated (D_0) and experimental bond dissociation energies [kcal mol^{-1}]

Bond	D_0[a]		Exptl[b]	Bond	D_0[a]		Exptl[d]
Sc^+-CH_3	59	60	65 ± 5, 59 ± 5[c]	H–H	102	104	104
HSc^+-CH_3	57	56	61 ± 5	CH_3-H	101	101	105
$Sc^+=CH_2$	86	87	97 ± 6[c]	C_2H_5-H	97	97	100
Sc^+-H	61	61	54 ± 4	C_3H_7-H	97	97	98
$CH_3Sc^+-CH_3$	57	58	57 ± 5	CH_3-CH_3	82	82	90
$Sc^+-C_2H_4$	34	35	40 ± 5	$CH_3-C_2H_5$	79	79	88
				$CH_2=CH_2$	168	169	174

[a] The first value was obtained at the B3LYP/6-311+G(d,p) level of theory, and the second at the B3LYP/6-311++G(3df,3pd) level. [b] The experimental data are from ref. [38] unless otherwise noted. [c] Ref. [39]. [d] Ref. [40].

From Table 1, we found that the calculated D_0 values for Sc^+-R species (where R denotes an organic fragment)

0947-6539/03/0902-0486 $ 20.00+.50/0 *Chem. Eur. J.* **2003**, *9*, No. 2

reproduce the experimental values. The errors introduced by calculations for the relative energies for different isomers are estimated to be ± 5 kcal mol^{-1} on the basis of our experience and that of others.[41, 42]

We also inspected the values of $\langle S^2 \rangle$ for all species involved in the reactions of Sc^+ with C_nH_{2n+2} ($n = 1-3$), and found the deviation of $\langle S^2 \rangle$ was less than 5%. This indicates that spin contamination was small in all calculations.

The above results lead us to conclude that the level of theory used in this work is capable of describing the basic electronic characteristics of the species of interest. In addition, the role of relativistic effects may be considered insignificant for [Sc, C_n, H_{2n+2}] ($n = 1-3$) systems. The effects on geometries and energies normally can be neglected for systems containing only first- and second-row elements, and this is also be true of the third-row elements, unless a very high accuracy is required. In present work our goal is to describe the interesting properties of the [Sc, C_n, H_{2n+2}] ($n = 1-3$) PESs and to give the relative energies of various species rather than their accurate total energies. It is expected that the errors due to relativistic effects could be almost equal for the various species involved in the reactions of Sc^+ with C_nH_{2n+2} ($n = 1-3$), and these errors would mostly cancel each other in the calculations of the relative energies. Therefore, we believe that errors resulting from relativistic effects are much less than those due to incomplete basis sets and can be safely neglected.

Reaction of Sc^+ with methane: Reactions of first-row transition-metal ions with methane were extensively studied by ion-beam techniques and by ion cyclotron resonance mass spectrometry in the late 1980s. All first-row transition-metal ions except for Mn^+ were observed to react with CH_4 with similar endothermicities.[43–52] At low energies, the most favorable reaction is dehydrogenation to form $MCH_2^+ + H_2$. The relevant reactions can be understood in terms of the general mechanisms shown in Scheme 1 (top). Elimination of H_2 proceeds via a four-center transition state or a metal dihydrido methylene cationic intermediate $M^+(H)_2CH_2$. The most detailed experimental results for the reactions of Fe^+[51] and Co^+,[52] including detailed reaction mechanisms and PESs, were reported by Armentrout et al. They found that the barriers of the reactions of Fe^+ and Co^+ with methane to yield $FeCH_2^+$ and $CoCH_2^+$ were associated with the four-centered transition state shown in Scheme 1 (top). Musaev et al. reported ab initio studies on the mechanisms of the reactions of $FeCH_2^+$ and $CoCH_2^+$ with H_2, and the reverse of the reactions of Fe^+ and Co^+ with CH_4.[11, 12] They identified the four-centered TS shown in Scheme 1 (top). More recently, they also studied the reaction mechanism of Sc^+ with CH_4 by using the CASSCF and MR-SDCI-CASSCF methods.[16]

To comprehensively research the reactions of the early first-row transition-metal ions with small alkanes such as CH_4, C_2H_6, and C_3H_8, and to calibrate the results given by Musaev et al. earlier, here we study the reaction of Sc^+ with CH_4 in detail by using DFT theory, including geometry optimization of various species involved on the PES of [Sc, C, H_4]$^+$, relative energies, and reaction mechanism. Optimized geometric parameters are shown in Figure 1. The electronic total energies and relative energies are listed in Table 2. The reaction process on the PES of [Sc, C, H_4]$^+$ is shown in Figure 2, and the PES of [Sc, C, H_4]$^+$ in Figure 3.

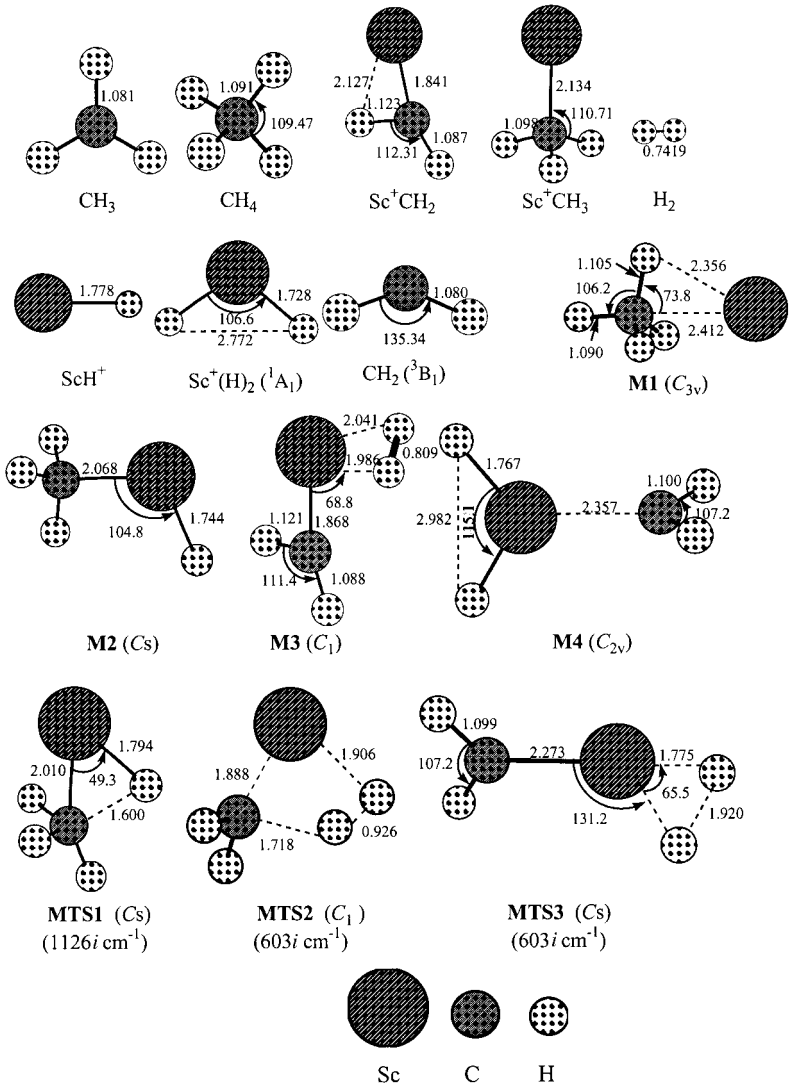

Figure 1. Optimized geometries [Å, °] of species involved in the reaction of Sc^+ with CH_4 at the B3LYP/6-311 + G(d,p) level of theory. The values in parentheses are the imaginary frequencies corresponding to the transition vectors.

Table 2. Electronic total energies E [hartree] and relative energies ΔE [kcal mol^{-1}] of the species involved in the reaction $Sc^+ + CH_4$ at different levels of theory.

Species	B3LYP/6-311 + G(d,p)		B3LYP/6 – 311 + G(3df, 3pd)		ZPE
	E	ΔE	E	ΔE	
$Sc^+ + CH_4$	– 800.913214	0.0	– 800.916689	0.0	27.96
M1	– 800.940021	– 16.09	– 800.945195	– 17.16	28.69
M2	– 800.930551	– 15.16	– 800.934947	– 15.74	23.68
M3	– 800.885690	12.56	– 800.890239	11.89	23.25
M4	– 800.798155	63.78	– 800.801821	63.66	19.54
MTS1	– 800.893344	8.02	– 800.897775	7.43	23.51
MTS2	– 800.884529	12.35	– 800.889211	11.59	22.31
MTS3	– 800.789774	68.63	– 800.793389	68.54	19.13
$Sc^+CH_3 + H$	– 800.834568	42.04	– 800.838782	41.58	20.65
$Sc^+H + CH_3$	– 800.837101	40.79	– 800.841108	40.46	20.99
$Sc^+CH_2 + H_2$	– 800.862913	23.04	– 800.870095	20.72	19.44
$Sc^+(H)_2(^1A_1) + CH_2(^3B_1)$	– 800.719257	98.07	– 800.724071	95.93	16.49

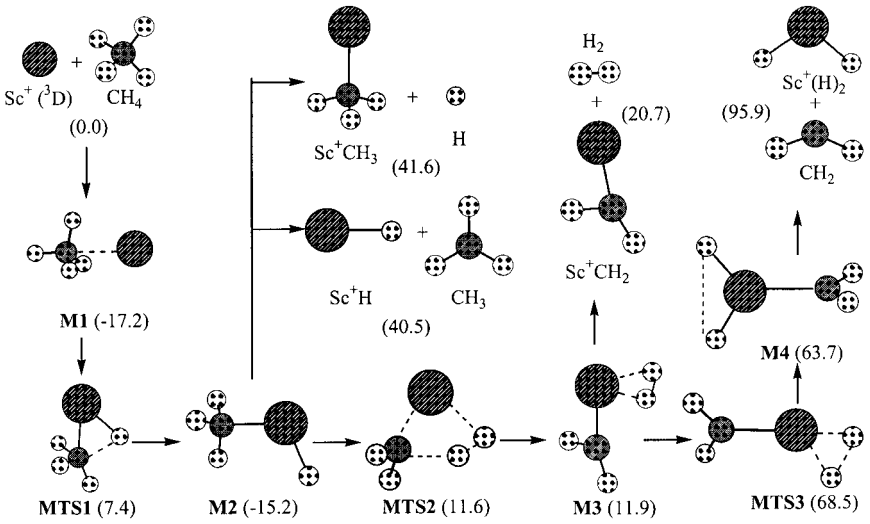

Figure 2. Reaction process on the PES of $[Sc, C, H_4]^+$, calculated at the B3LYP/6-311 + + G(3df,3dp)//B3LYP/6-311 + G(d,p) level of theory. The values in parentheses are the energies [kcal mol^{-1}] relative to the separate reactants.

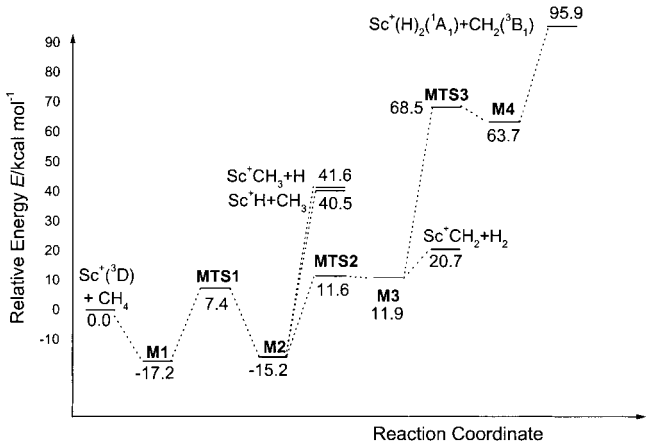

Figure 3. The PES for the reaction of Sc^+ with CH_4, calculated at the B3LYP/6-311 + + G(3df,3dp)//B3LYP/6 – 311 + + G(d,p) level of theory.

Four minima **M1** – **M4** and three first-order saddle points **MTS1** – **MTS3** are located along the reaction path (Figure 1). Initially, the ion – molecule complex **M1** is formed as $Sc^+(^3D)$ and CH_4 approach each other. The ground state of this complex is a triplet and has C_{3v} symmetry. This result agrees with that found by Musaev and Morokuma.[16] It is calculated to be 17.2 kcal mol^{-1} more stable than the $Sc^+(^3D) + CH_4$ entrance channel. The singlet state of **M1** is less stable than the triplet state by 13.3 kcal mol^{-1}. Along the reaction coordinate lies the C–H insertion species **M2** [i.e., $Sc^+(H)(CH_3)$], the key intermediate in this reaction, which is 15.2 kcal mol^{-1} more stable than the original entrance channel and lies 2.0 kcal mol^{-1} above **M1**. As expected, **M2** has C_s symmetry, and its ground state is a singlet. Thus, we conclude there must be effective spin – orbit coupling interactions that allow intersystem crossing from the triplet to the singlet state during insertion of Sc^+ into the C–H bond to lead the system to the energetically most favorable PES. Minima **M1** and **M2** are connected by the C–H bond-insertion transition state **MTS1**. We tried to optimize its geometries in both the singlet and triplet states, but only the structure of the singlet state was located, and the triplet state was not found, despite careful searches. We also optimized the triplet geometry of **MTS1** at the MP2/6-311 + G(d,p) level of theory, but this was also unsuccessful. This indicates that the intersystem crossing could occur prior to the appearance of the saddle point. As shown in Figure 1, **MTS1** has a three-membered-ring TS structure in which the C–H bond is breaking and the C-Sc-H bridging structure is forming. The C–H bond in **MTS1** is elongated by 0.495 Å and the Sc^+–C and Sc^+–H lengths are shortened by 0.402 and 0.562 Å relative to those in **M1**. This TS structure is characterized by an imaginary frequency of 1126*i* cm^{-1}, and the transition vector corresponds to the expected components of the reaction coordinate in which Sc^+ is inserting into the C–H bond. The barrier height from **M1** to **MTS1** is calculated to be 24.6 kcal mol^{-1}.

Minimum **M2** can directly decompose by breaking of the Sc^+–C bond to form Sc$^+$H and a CH_3 radical. Competing with this process is the cleavage of the Sc^+–H bond to yield Sc^+CH_3 and an H atom. Our calculations indicate these two processes have similar energy requirements (see Figure 3). Minimum **M2** can be also converted to the next minimum structure on the PES of $[Sc, C, H_4]^+$, **M3**, which is a precursor from which molecular hydrogen will be eliminated. It lies 11.9 kcal mol^{-1}

0947-6539/03/0902-0488 $ 20.00+.50/0 *Chem. Eur. J.* **2003**, *9*, No. 2

above the entrance channel. As shown in Figure 1, **M3** has a C_1-symmetric structure in which an H_2 unit is bound to an Sc^+CH_2 moiety by primarily electrostatic interaction. Note that the geometry of **M3** is very different from those given early by Musaev et al.[11, 12, 16] for the corresponding adducts of Fe^+CH_2, Co^+CH_2, and Sc^+CH_2 with H_2, which have C_{2v} symmetry and a coplanar structure. In the present calculations, the geometric parameters of the $ScCH_2^+$ and H_2 units in **M3** resemble those of the free species. Minima **M2** and **M3** are connected by the saddle point **MTS2**, which lies 11.6 kcal mol^{-1} above the reactants. The structure of this transition state is similar to that of **M3**, and indicates that **MTS2** is very loose. As a result, the energy of **MTS2** is only 0.3 kcal mol^{-1} above **M3**. The barrier height from **M2** to **MTS2** is 26.8 kcal mol^{-1}, slightly higher by 2.2 kcal mol^{-1} than that of the initial C–H bond activation. Saddle point **MTS2** is a four-membered-ring TS corresponding to the activation of the second C–H bond in CH_4 and formation of H_2, similar to the case of the [M, C, H_4]$^+$ PES given by Musaev and Morokuma[16] earlier. The imaginary frequency of this TS is 603*i* cm^{-1}. The associated normal mode corresponds to motions of two hydrogen atoms.

Proceeding along the reaction coordinate, **M3** can decompose directly into the products $ScCH_2^+ + H_2$, and this channel is confirmed to be the lowest energy process on the PES, endothermic by 20.7 kcal mol^{-1}. Alternatively, **M3** can be converted to **M4**, a minimum corresponding to the metal dihydrido methylene cation intermediate proposed in Scheme 1 (top). In **M4**, Sc^+ has inserted into the H–H bond. It has C_{2v} symmetry (Figure 1) with two perpendicular planes formed by $Sc(H)_2^+$ and CH_2 units. Although **M4** is less stable by 63.7 kcal mol^{-1} than the entrance channel, it is a stable structure, as confirmed by vibrational analysis. Direct dissociation of **M4** leads to the dihydrido species $Sc^+(H)_2$ and a methylene radical. This dihydrido species has, in fact, been observed by Bushnell et al.[53] However, stable dihydrido species similar to **M4** were not found for $Co^+(H)_2$ and $Fe(H)_2^+$ in previous studies by Holthausen et al.,[13–15] Musaev et al.,[11, 12] and Bauschlicher et al.[54] These earlier studies did not support the presence of such dihydrido species in the reactions of late first-row transition-metal ions with alkanes. This can be understood in terms of differences in $D_0(M^+–H)$. For Fe^+ and Co^+, the D_0 values are 49 and 46 kcal mol^{-1}, respectively, while $D_0(Sc^+–H)$ is 61 kcal mol^{-1}. The higher D_0 value could be responsible for the existence of the dihydrido species $Sc(H)_2^+$ in the reactions of Sc^+ with alkanes.

Minima **M3** and **M4** are connected by the saddle point **MTS3**, in which Sc^+ is inserting into the H–H bond. The TS has C_s symmetry, and its relative energies with respect to **M3** and **M4** are 56.6 and 4.8 kcal mol^{-1}, respectively. Evidently, this process is only available under high-energy conditions. Compared to the structure of **M3**, the H–H and C–Sc distances in **MTS3** are significantly longer, but the CH_2 unit remains almost unchanged. The imaginary frequency for this TS is 603*i* cm^{-1}. The exit channel of **M4** is formation of $Sc^+(H)_2$ and CH_2, which is endothermic by 95.9 kcal mol^{-1} relative to the entrance channel.

From Figure 2, it is clear that the H_2 elimination reaction is the most energetically favorable channel under low-energy conditions; it consists of two elementary steps: oxidative addition of the C–H bond to the metal center to form $Sc^+(H)(CH_3)$ and rearrangement of the insertion product. Our calculations indicate that the energy demand of the rearrangement process is slightly higher than that of the initial C–H activation. This result is in qualitative agreement with earlier experimental findings.

Reaction of Sc^+ with ethane: Tonkyn et al. found that C_2H_6 reacts with all first-row transition-metal ions, except for Mn^+ in 100 Pa of He.[4] The main products are listed in Equations (4)–(9). To explain the earlier experimental results and to generalize the mechanism postulated in Scheme 1 (middle), Holthausen et al. reported two examples of theoretical investigations on the reactions of the late first-row transition-metal ions Fe^+ and Co^+ with ethane.[13, 14] Their calculations indicated that: 1) These reactions process along both the C–C and C–H activation branches; 2) Each branch is composed of two elementary steps: C–C or C–H bond activation and subsequent isomerization of the inserted species by a β-H shift; 3) The rate-determining steps of the two branches are the isomerizations of the intermediate insertion products, rather than the initial C–C or C–H activation.

Two questions arise: 1) Is a reaction mechanism similar to that of late first-row transition-metal ions with ethane also applicable to early first row transition ions? 2) Do other reaction channels exist for the reactions of early first-row transition-metal ions with ethane? To answer these questions, we studied the reactions of Sc^+ with ethane in detail. After careful searching, we found two new reaction channels: 1,1-H_2 elimination and concerted elimination of CH_4, in which C–C and C–H bonds are activated synchronously with a higher activation barrier than the individual C–C and C–H activation channels.

Double-dehydrogenation mechanisms in the reactions of M^+ (M = Fe, Co) with C_2H_6 to form $MC_2H_2^+ + 2H_2$ were not reported in earlier studies by Holthausen et al.[13, 14] However, spontaneous double dehydrogenation was observed experimentally in the reactions of first-row transition-metal ions such as Sc^+ and Ti^+ with ethane.[55] Hence we also investigated double-dehydrogenation mechanism in the reaction of Sc^+ with C_2H_6.

Our calculations located ten intermediates **E1**–**E10** and eleven first-order saddle points **ETS1**–**ETS11** on the PES of [Sc, C_2, H_6]$^+$. Their main geometric parameters are shown in Figures 4 and 5, respectively.

Intermediate **E1** is an initial ion–molecule complex formed when $Sc^+(^3D)$ and C_2H_6 approach each other. Similar to the initial adduct of Sc^+ with methane **M1**, the ground state of **E1** is also a triplet, and it is 16.2 kcal mol^{-1} more stable than the isolated reactants. The corresponding singlet state is 13.2 kcal mol^{-1} less stable. This complex has C_2 symmetry, similar to those of the ethane complexes of Cu^+ and Co^+ given by Rosi et al.[56] and Holthausen and Koch,[13] but unlike those of the ethane complexes of Cr^+, Fe^+, Ni^+, and Mo^+, which have C_s symmetry.[14, 56, 57] The C_2H_6 unit in **E1** remains almost undisturbed compared to free C_2H_6, and this indicates that the interaction between Sc^+ and C_2H_6 is essentially electrostatic,

  0947-6539/03/0902-0489 $ 20.00+.50/0

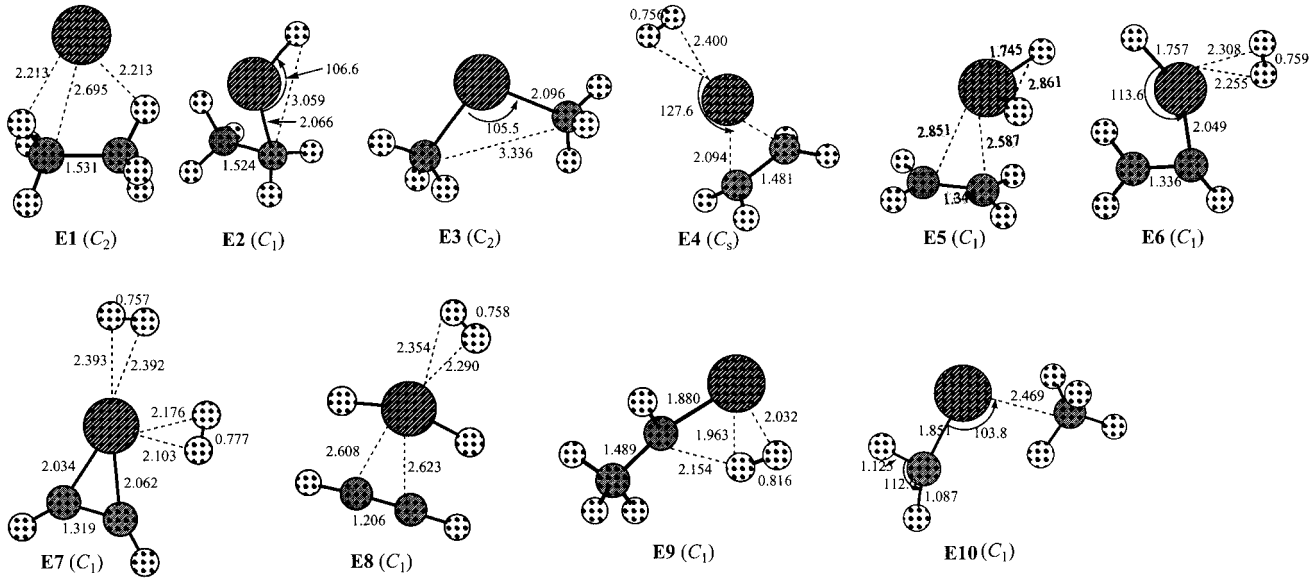

Figure 4. Optimized geometrical parameters [Å, °] for the intermediates on the PES [Sc, C_2, H_6]$^+$ at the B3LYP/6–311 + G(d,p) level of theory.

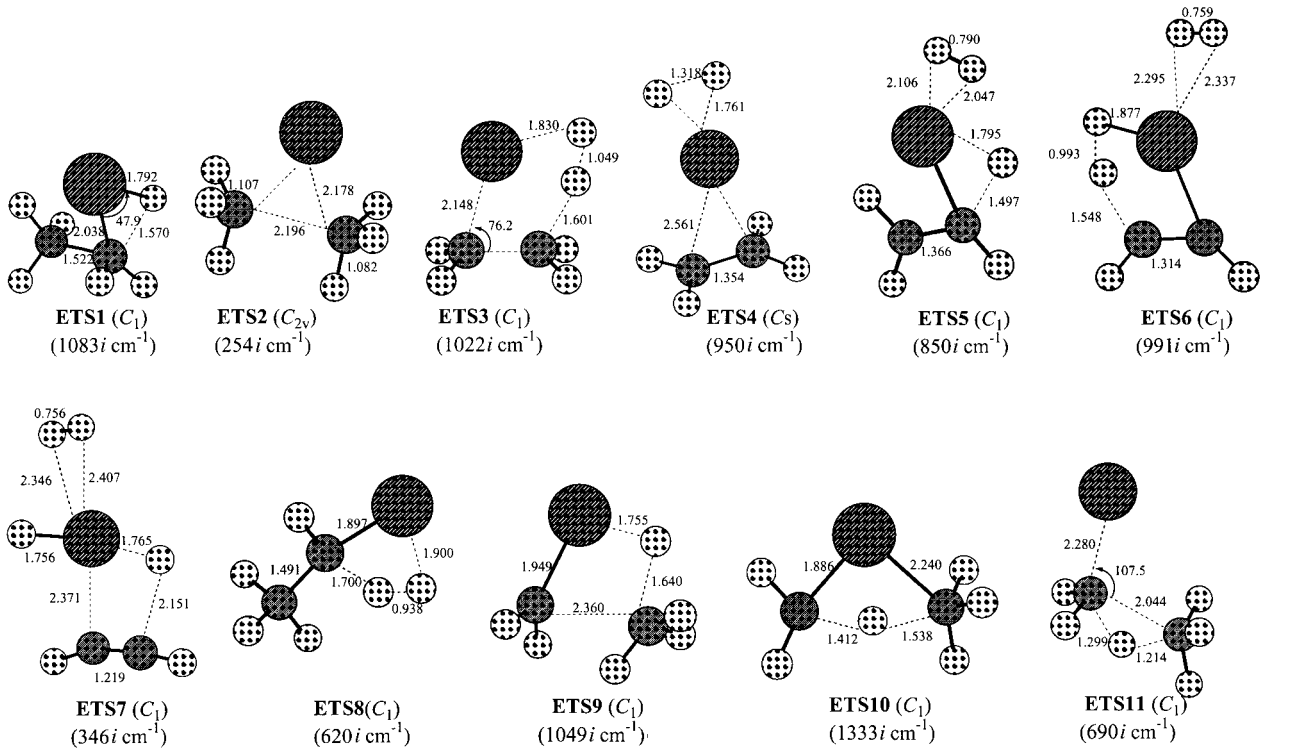

Figure 5. Optimized geometries [Å, °] for the first-order saddle points on the PES of [Sc, C_2, H_6]$^+$ at the B3LYP/6-311 + G(d,p) level of theory. The values in parentheses are the imaginary frequencies corresponding to the transition vectors.

as evidenced by the long distance between Sc^+ and C or H atoms. Our calculations indicate that **E1** is a common initial adduct for three subsequent activation branches: C–C bond activation, C–H bond activation, and synchronous C–C and C–H bond activations.

Reaction channels following initial C–H bond activation:

The C–H bond activation branch on the PES of [Sc, C_2, H_6]$^+$ starts from the initial ion – molecule complex **E1**. Along the reaction coordinate, **E1** can be converted to the C–H inserted species **E2** via the C–H activation transition state **ETS1**. This C–H inserted species is calculated to be 7.2 kcal mol^{-1} more stable than **E1**. We attempted to optimize the saddle points of both singlet and triplet states of the C–H inserted species, but only the saddle point for the singlet state of **ETS1** was located. Despite numerous attempts to locate a triplet state for C–H bond activation, the input structures all collapsed into **E1** or **E2**. This is similar to the insertion of Sc^+

0947-6539/03/0902-0490 $ 20.00+.50/0 *Chem. Eur. J.* **2003**, *9*, No. 2

into a C–H bond of methane, and indicates that intersystem crossing between triplet and singlet could occur before the saddle point. Saddle point **ETS1** has C_1 symmetry, and the transition vector associated with the imaginary frequency of $1083i$ cm^{-1} confirms it as the correct saddle point for the C–H bond insertion process. The breaking C–H bond is elongated to 1.570 Å in **ETS1**.

Once **E2** is formed, it can follow various possible channels by decomposition or isomerization. We found that five channels I–V are accessible to **E2**. Channel I involves β-H migration to form the intermediate **E4** via the saddle point **ETS3**, in which the breaking C–H bond is elongated to 1.601 Å and the forming H–H bond is shortened to 1.049 Å. The imaginary frequency of **ETS3** is $1022i$ cm^{-1}. Note that **E4** is a complex between cationic scandium–ethylene and molecular hydrogen, in which the H–H bond length resembles that of free H_2. This complex differs from species **C** in Scheme 1 (middle), the generally proposed dihydrido species in which the metal ion has already inserted into the H–H bond. Although we also found such a minimum on the PES of $[Sc, C_2, H_4]^+$, denoted **E5**, this dihydrido species is formed after **E4** and is 15.6 kcal mol^{-1} less stable than **E4**. Intrinsic reaction coordinate (IRC) analysis confirmed that the forward product from **ETS3** is **E4** rather than **E5**. This TS involves a five-membered-ring structure. The barrier height from **E2** to **ETS3** is 16.5 kcal mol^{-1}, almost equal to that of the first C–H bond activation.

Along the reaction coordinate, we found that three paths i–iii are open to **E4**, as shown in Figure 6. Path i is direct dissociation of **E4** to form $H_2 + Sc(C_2H_4)^+$ (1,2-H_2 elimination). This path is exothermic by 5.3 kcal mol^{-1} relative to the reactants, and it is the energetically most favorable reaction channel. This result is in good agreement with earlier experimental finding. Path ii involves the isomerization of **E4** to dihydrido species **E5** via saddle point **ETS4** with a barrier of 17.4 kcal mol^{-1}. Intermediate **E5** is only 2.3 kcal mol^{-1} more stable than **ETS4**. The imaginary frequency associated with the transition vector of **ETS4** is $950i$ cm^{-1}. As shown in Figure 5, it is an H–H inserted transition state. The exit channel of **E5** is formation of $Sc^+(H)_2 + C_2H_4$, which is endothermic by 20.1 kcal mol^{-1} relative to the entrance channel, and energetically less favorable than the 1,2-H_2 elimination path i. Path iii is responsible for the double dehydrogenation reaction [Eq. (7)]. Along the pathway, another C–H activation TS, **ETS5**, follows **E4**. In this TS the length of the breaking C–H bond is 1.497 Å. Its imaginary frequency is $850i$ cm^{-1}. The barrier height from **E4** to **ETS5** is

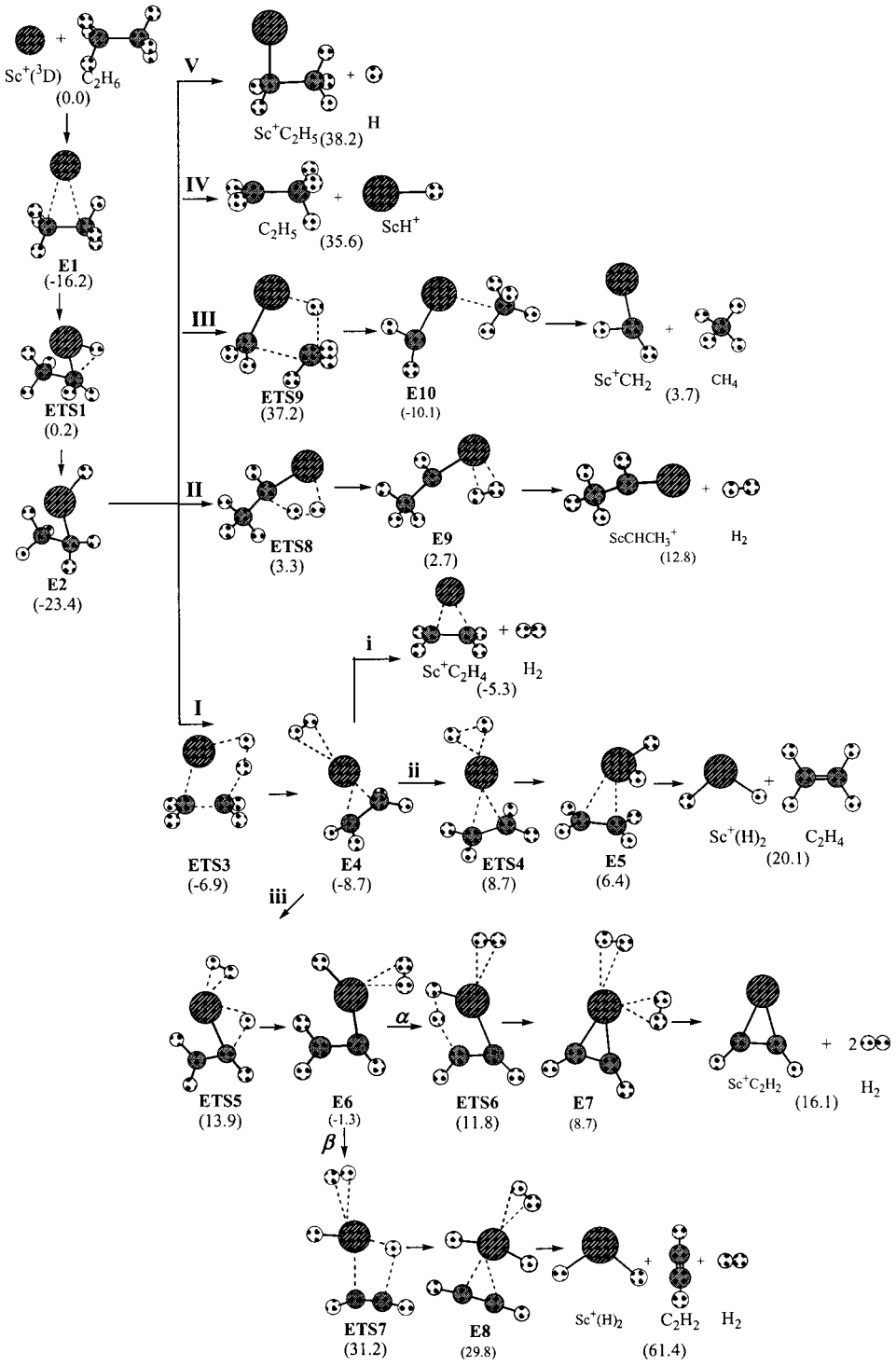

Figure 6. Reaction process following initial C–H activation for the reaction of Sc^+ with C_2H_6.

  0947-6539/03/0902-0491 $ 20.00+.50/0

22.6 kcal mol^{-1}. The IRC calculations indicate that the forward product from **ETS5** is the intermediate **E6**, a complex between molecular hydrogen and the product of C–H insertion of Sc^+ into ethane. Two product paths ***α*** and ***β*** leading from **E6** were located. Path ***α*** is the double dehydrogenation reaction, which also involves a β-H migration transition state, **ETS6**, similar to the 1,2-H_2 elimination path mentioned above. This TS lies 11.8 kcal mol^{-1} above the entrance channel and is 18.7 kcal mol^{-1} less stable than **ETS3**, the first-order saddle point of the first β-H migration. This indicates that in the reaction of Sc^+ with ethane double dehydrogenation is more difficult than 1,1-H_2 and 1,2-H_2 elimination. The forward product from **ETS6** is the intermediate **E7**, a productlike complex whose exit channel is $ScC_2H_2^+ + 2H_2$, endothermic by 16.1 kcal mol^{-1} relative to the entrance channel. Path ***β*** also involves β-H migration, via **ETS7** with an imaginary frequency of 346*i* cm^{-1}. However, the geometry of **ETS7** is very different from that of **ETS6**. In the former, Sc^+ is bonded to the two H atoms, whereby the geometry of the $Sc^+(H)_2$ unit is close to that of the corresponding free species. In the latter, the second hydrogen molecule is forming. Our calculations indicate that **ETS7** is 31.2 kcal mol^{-1} higher in energy than the separate reactants, and 19.4 kcal mol^{-1} less stable than **ETS6**. So path ***β*** will be accessible only under high-energy conditions. An IRC calculation was performed from **ETS7**, and the forward product is intermediate **E8**, an additive complex composed of the three species $Sc^+(H)_2$, H_2, and C_2H_2, whose direct dissociation into three fragments requires 61.4 kcal mol^{-1}.

The second pathway from **E2** (pathway II) also involves an H-migration transition state, **ETS8**. This TS has some similarity to **ETS3**, in that the β-H migration in **ETS3** is replaced by a α-H migration. Transition state **ETS8** is a four-membered-ring TS, with a barrier of 26.7 kcal mol^{-1}, 10.2 kcal mol^{-1} higher than that of β-H migration. The forward product of **ETS8** is intermediate **E9**, a complex of ethyl scandium carbene cation with molecular hydrogen, whose dissociation also leads to loss of H_2. This H_2 loss channel is referred as 1,1-H_2 elimination, as opposed to the 1,2-H_2 elimination mentioned above. This channel is endothermic by 12.8 kcal mol^{-1}.

The third reaction channel from **E2** (pathway III), involves the four-centered TS **ETS9**, in which the C–C bond is breaking and the H atom bound to the scandium atom is migrating to the methyl carbon atom (see Figure 5). The IRC calculations from this TS, following the transition vector in both directions, indicate that it connects **E2** and **E10**, a complex of scandium carbene cation with methane. Both the methane moiety and the scandium carbene unit in **E10** are only slightly distorted compared to the geometric parameters of free CH_4 and Sc^+CH_2 in Figure 1. The geometry of **E10** is different from those of the corresponding complexes of Co^+CH_2 and Fe^+CH_2 with CH_4 found earlier,[12,13] which have C_{2v} and C_s symmetries, respectively, and C-Co-C and C-Fe-C angles of 180.0°. The methane unit in **E10** is coordinated to the Sc^+CH_2 species in an η^3 fashion with a C-Sc-C angle of 103.8°. Its energy is 10.1 kcal mol^{-1} lower than the energy of the separate reactants. The barrier height from **E2** to **ETS9** is 60.6 kcal mol^{-1}, which is much higher than for channels I and II discussed above. Therefore, the process is highly disadvantageous from an energetic viewpoint. The dissociation of **E10** can lead to the loss of CH_4, which requires a energy of 13.8 kcal mol^{-1}. This indicates that CH_4 loss from the reaction of $Sc^+ + C_2H_6$ could occur along the initial C–H bond activation branch. This reaction mechanism is presented for the first time on the PES of $[Sc, C_2, H_6]^+$. Similar cases were not found in the reactions of Fe^+ and Co^+ with ethane.[13,14] Although this CH_4 elimination channel is energetically less favorable at low energy, it could be an alternative path for the CH_4 loss mechanism proposed in Scheme 1 (middle) under high-energy conditions.

The last two channels from **E2** (channels IV and V) are direct fragmentation processes with rupture of the Sc–C bond to form $Sc^+H + C_2H_5$ or of the Sc–H bond to form $Sc^+C_2H_5 + H$. These two processes are endothermic by 35.6 and 38.2 kcal mol^{-1}, respectively, and require almost equal energy (see Figure 6). The high-energy requirements indicate these two processes are energetically less favorable under low-energy conditions.

The reaction process along the initial C–H activation branch for the reaction of Sc^+ with C_2H_6 is summarized in Figure 6, and the corresponding energetic profile is shown in Figure 7.

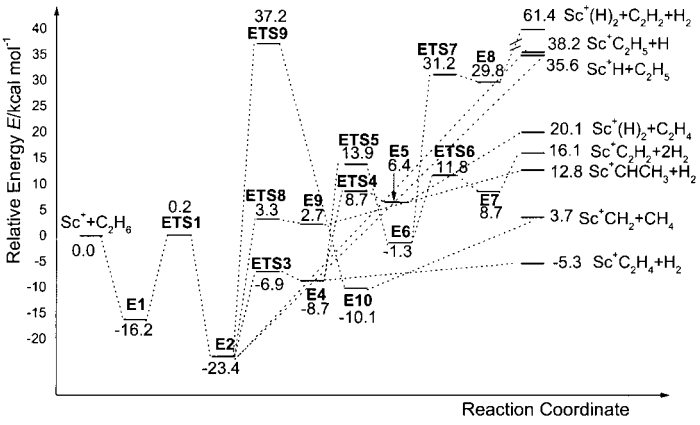

Figure 7. Energetic profile along the initial C–H activation branch in the reaction of Sc^+ with C_2H_6.

From Figure 7, it is clear that 1,2-H_2 elimination is energetically most favorable at low energy along the initial C–H activation channel for the reaction of Sc^+ with C_2H_6. The rate-determining step for this channel is the initial C–H activation. This is in contrast with the 1,2-H_2 losses in the reactions of Fe^+ and Co^+ with ethane, where the energetic bottleneck is the isomerization of the C–H inserted species.

Reaction channels following initial C–C bond activation: Along the C–C bond activation branch, the next minimum structure after the initial complex **E1** is intermediate **E3**, a dimethyl species in which Sc^+ has inserted into the C–C bond. The inserted species has C_2 symmetry and, as expected, its ground state is a singlet, with a relative energy 35.1 kcal mol^{-1} below that of the separate reactants. Note that **E3** is an overall minimum on the PES of $[Sc, C_2, H_6]^+$. Intermediates **E1** and

0947-6539/03/0902-0492 $ 20.00+.50/0 *Chem. Eur. J.* **2003**, *9*, No. 2

E3 are connected by the first saddle point **ETS2**, which corresponds to C–C bond activation with an activation barrier of 26.3 kcal mol^{-1}. The ground state of **ETS2** is a triplet with an energy 4.9 kcal mol^{-1} lower than than that of the corresponding singlet state. So we conclude there must be effective spin–orbit coupling interactions that allow intersystem crossing from the triplet to the singlet after **ETS2**. The energy of **ETS2** is 9.9 kcal mol^{-1} higher than that of **ETS1**, the C–H activation TS. Thus, from a purely energetic point of view, C–C bond activation is less favorable than C–H bond activation. We found that **ETS2** has a C_{2v}-symmetric structure in which the C–C distance is elongated by 0.665 Å and the Sc–C distance is shortened by 0.417 Å relative to **E1**. From these parameters it is clear that **ETS2** is a three-membered-ring transition state. The imaginary frequency of this saddle point is 254*i* cm^{-1}, and the corresponding transition vector indicated by vibration analysis corresponds to the breaking of the C–C bond and the reorientation of the methyl groups.

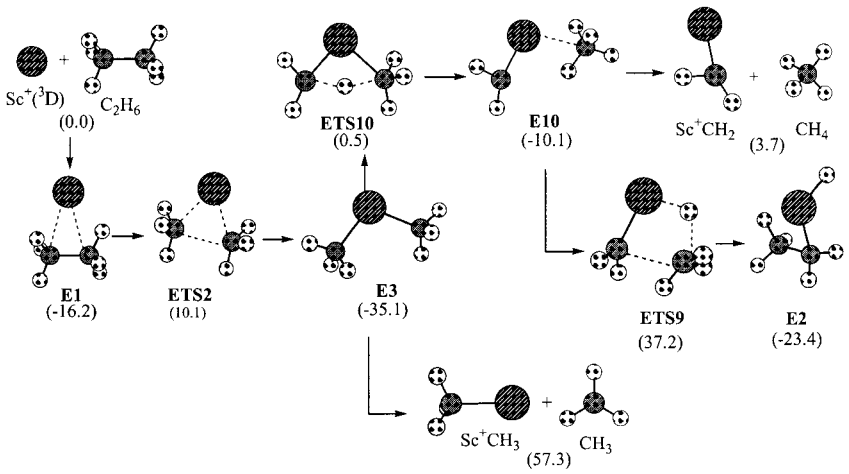

Figure 8. Reaction process following initial C–C bond activation for the reaction of Sc^+ with C_2H_6.

Once **E3** is formed, it can follow two possible production channels immediately by isomerization or decomposition. The direct rupture of the Sc–C bond in **E3** can lead to $Sc^+CH_3 + CH_3$, as proposed in Scheme 1 (middle). The process is endothermic by 57.3 kcal mol^{-1}. The isomerization of **E3** is an energetically more favorable reaction path which involves three-center transition state **ETS10**. As shown in Figure 5, **ETS10** is an H-migration transition state on the PES, in which a hydrogen atom is moving from one carbon atom to the other, and lengths of the breaking and forming C–H bonds are 1.412 and 1.538 Å, respectively. The corresponding imaginary frequency is 1333*i* cm^{-1}. Vibration analyses also showed that the corresponding transition vectors are completely consistent with the notion of 1,3-H migration. The relative energy of **ETS10** is 0.5 kcal mol^{-1} above the entrance channel. The forward product from **ETS10** is **E10**. Once **E10** is formed, two possible channels are open. One is its direct dissociation to form $ScCH_2^+(^1A) + CH_4$, which requires 13.8 kcal mol^{-1}, and the overall reaction $Sc^+(^3D) + C_2H_6 \rightarrow ScCH_2^+(^1A) + CH_4$ is endothermic by 3.7 kcal mol^{-1}. The other is the isomerization of **E10** to form the C–H inserted species **E2** via the four-membered-ring TS, **ETS9**. Evidently, in this case the C–C activation branch has already crossed into the C–H activation branch, and the subsequent process has been analyzed above. The reaction process along the C–C activation branch is shown in Figure 8, and the corresponding energetic profile in Figure 9.

From Figure 9, we note that the initial C–C bond activation is an energetic bottleneck for CH_4 loss at low energy in the reaction of Sc^+ with C_2H_6. This is similar to the 1,2-H_2 loss from $Sc^+ + C_2H_6$, but different from CH_4 loss from the reactions of Fe^+ and Co^+ with C_2H_6.[13, 14]

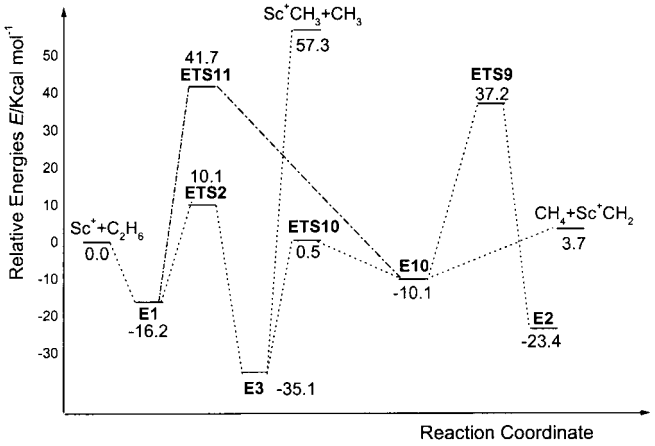

Figure 9. Energetic profile along the initial C–C bond activation branch (••••) and the synchronous C–C and C–H activation branch (•–•–) for the reaction of Sc^+ with C_2H_6.

Reaction channels following synchronous C–H and C–C activation: The C–C and C–H activation mechanisms of ethane by Sc^+ discussed above are both addition–elimination mechanisms which involve two consecutive elementary steps: oxidative addition of the C–C or C–H bond to the metal center and subsequent reductive elimination of small molecules. However, we also found another new reaction channel involving concerted C–C and C–H activation. The three-membered-ring TS **ETS11** was identified as a transition structure by one imaginary frequency of 690*i* cm^{-1}. From the geometries of **ETS11** (Figure 5), it is clear that the new mechanism is a radical substitution reaction in which attack of Sc^+ at a C atom of ethane leads to C–C bond activation and cleavage. This resembles closely the nucleophilic substitution mechanism for C–Cl bond activation found by Bickelhaupt et al.[58] However, in the latter case, the chloride leaving group coordinates to the metal atom, whereas in the present case the methyl leaving group abstracts a hydrogen atom from the methyl group. The transition vector of **ETS11** corresponds to the expected components of the reaction coordinate: breaking of the C–C bond and migration of the H atom from one C

  0947-6539/03/0902-0493 $ 20.00+.50/0

atom to the other. The ground state of this TS is a triplet, and thus differs from the C–C and C–H activation TSs, the ground states of which are singlets. The relative energy of **ETS11** is 41.7 kcal mol^{-1} above the entrance channel, and the corresponding singlet state is 10.3 kcal mol^{-1} less stable. To confirm connection of two minima by **ETS11**, a careful IRC calculation starting from this TS was performed along both the forward and reverse directions on the triplet PES of [Sc, C_2, H_6]$^+$. The calculated results indicate that the forward direction leads to the triplet state of **E10**, while the reverse direction leads to **E1**. However, since the ground state of **E10** is a singlet, intersystem crossing could occur in the course of the conversion of **ETS11** to **E10**. The activation energy from **E1** to **ETS11** is 57.9 kcal mol^{-1}. Although this process requires much higher energy than the consecutive C–C and C–H activation processes, it could be an alternative pathway for C–C and C–H activation under high-energy conditions. Similar to the C–C activation branch, this concerted activation branch can also cross into the C–H bond activation branch by isomerization of **E10**. The reaction process starting from the concerted pathway is shown in Figure 10, and the corresponding energetic profile in Figure 9.

In summary, the calculations show that three activation branches for the reaction of Sc$^+$ with C_2H_6 are available along the reaction coordinate: C–H activation, C–C activation, and synchronous C–H and C–C activation. Detailed mechanisms

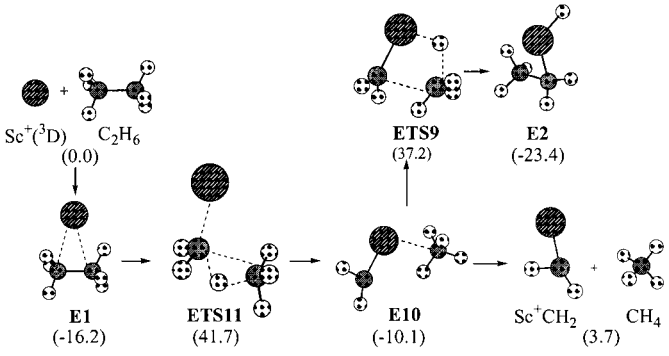

Figure 10. Reaction process following synchronous C–C and C–H activation for the reaction of Sc$^+$ with C_2H_6.

of reductive eliminations of H_2 and CH_4 from the reaction of Sc$^+$ with C_2H_6 were also elucidated. The loss of H_2 starts with C–H activation, and under low-energy conditions it proceeds according to a 1,2-H_2 addition–elimination mechanism in which the energetic bottleneck is the isomerization of the C–H inserted species, while under the high-energy conditions the 1,1-H_2 addition–elimination mechanism could be a alternative path for the loss of H_2. Double dehydrogenation in the reaction of Sc$^+$ with C_2H_6 is less energetically favorable than single H_2 elimination. The loss of CH_4 can proceed via all three activation branches. The energetically most favorable branch for CH_4 loss starts with initial C–C bond activation followed by the 1,3-H migration, which is the energetic bottleneck. The next most favorable path starts from C–H bond activation followed by isomerization of the C–H inserted species, and the least favorable path is synchronous C–C and C–H bond activation.

Reaction of Sc$^+$ with C_3H_8: The reactions of atomic transition-metal ions with propane have been paid more attention, because propane is the smallest alkane for which exothermic reactions are observed at thermal energies.[39] Although more experimental and theoretical studies have been devoted to the reactions of transition-metal ions with propane than any other hydrocarbon,[6–8, 15, 59–60] they focused on several late transition-metal ions. As far as we know, no theoretical study is available on the reactions of early transition ions with propane. Here we present a detailed study on the reaction of Sc$^+$ with C_3H_8.

Regardless of the complexity of the reaction $M^+ + C_3H_8$, the mechanisms proposed in Scheme 1 (bottom) are similar to those of the reactions of M^+ with CH_4 and C_2H_6 in many respects, that is, most of them involve C–C and C–H bond cleavage to form various smaller neutral molecules and fragment ions. Moreover, our detailed studies confirmed that the mechanisms found in the reactions of Sc$^+$ with CH_4 and C_2H_6 generally apply to the reaction $Sc^+ + C_3H_8$. In this section, we describe the detailed reaction mechanisms of $Sc^+ + C_3H_8$, and only particular characteristics that are different from the reactions of Sc$^+$ with CH_4 and C_2H_6 are discussed further.

The reaction of Sc$^+$ with propane can start along four branches: C–C activation, primary C–H activation, secondary C–H activation, and synchronous C–C and C–H activation. Along the four activation branches various intermediates and the first-order saddle points on the PES of [Sc, C_3, H_8]$^+$ are located. The optimized structures of various intermediates and transition states involved in the reaction $Sc^+ + C_3H_8$ are shown in Figures 11 and 12, respectively. The reaction process schemes and the corresponding PESs along the four activation branches are shown in Figures 13–20.

Initially, the interaction between Sc$^+$ and C_3H_8 occurs as they approach one another to form an ion–molecule addition complex. Three stable minima **P1**–**P3** for the initial complex are found on the PES of [Sc, C_3, H_8]$^+$. This differs from the corresponding adducts of Fe$^+$[15] and Ni$^+$[59] with C_3H_8, for which only one minimum is found in each case. Minima **P1**, **P2**, and **P3** have C_{2v}, C_1, and C_s symmetry, respectively, as shown in Figure 11. Their ground states are all triplets. As expected, however, the ground states of both C–C and C–H inserted species and subsequent species on the PES lie on the corresponding singlet surface. Hence, intersystem crossing between the singlet and triplet PESs must take place in the oxidative addition of the C–C or C–H bond to the metal center.

Reaction pathway following initial C–C activation: The detailed mechanism along the initial C–C activation branch is shown in Figure 13. Intermediate **P1** is a Sc$^+$ propane complex, which acts as a precursor of C–C activation. The propane unit in this complex is almost undisturbed compared to free propane. This intermediate can be converted to the C–C inserted species **P4** via the C–C cleavage transition state **PTS1**. The ground state of this TS is a triplet, and it lies 7.3 kcal mol^{-1} above the separate reactants. The corresponding singlet is 6.9 kcal mol^{-1} less stable. The C–C distance in the ground state TS is elongated to 1.957 Å, and the corresponding transition vector indicated by vibration analysis corre-

0947-6539/03/0902-0494 $ 20.00+.50/0 *Chem. Eur. J.* **2003**, *9*, No. 2

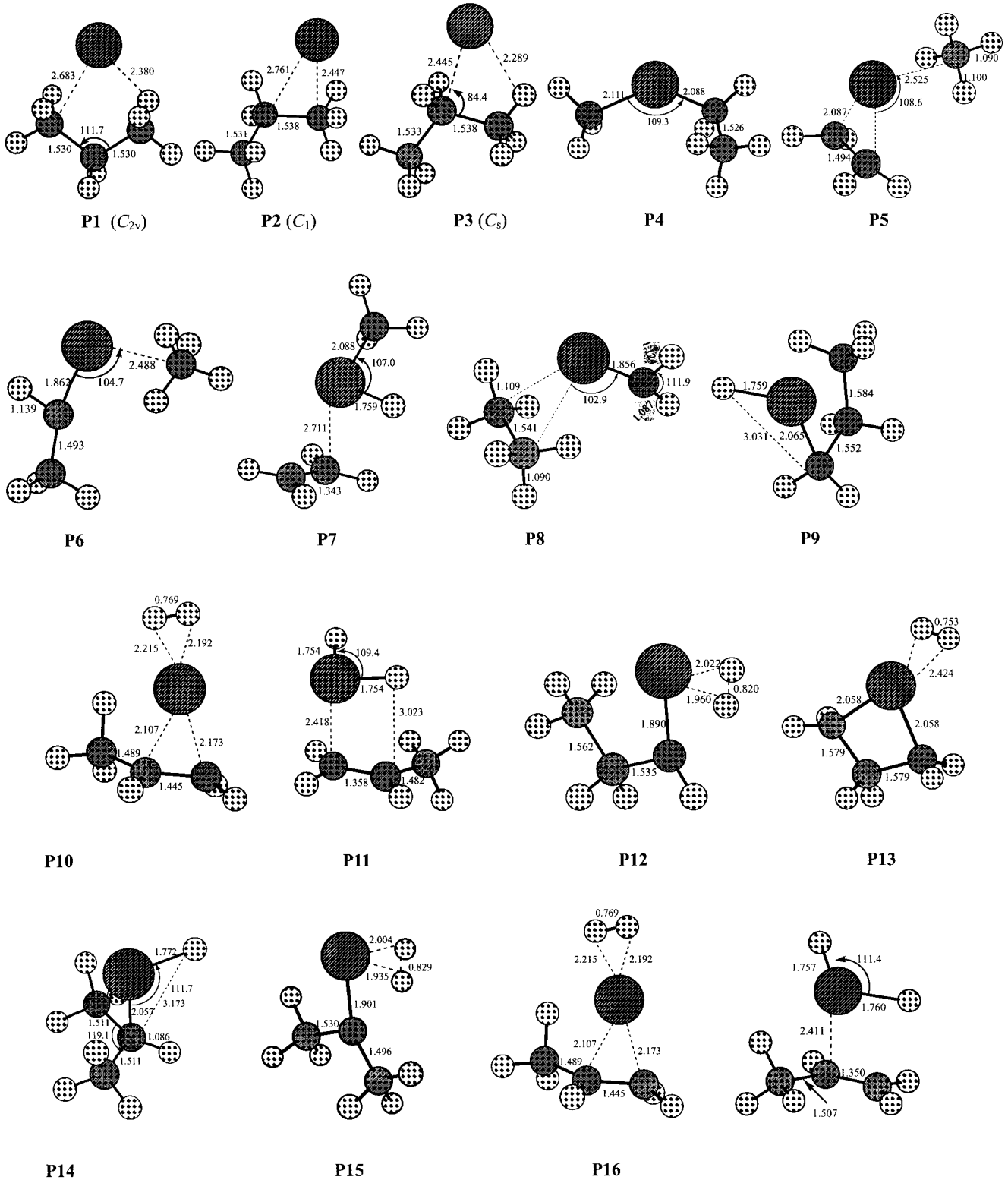

Figure 11. Optimized geometrical parameters [Å, °] for the intermediates on the PES [Sc, C_3, H_8]$^+$ at the B3LYP/6-311 + G(d,p) level.

sponds to the breaking of the C–C bond and reorientation of the methyl groups. The imaginary frequency of the saddle point is 323*i* cm^{-1}. The barrier height from **P1** to **P4** is 29.2 kcal mol^{-1}. Once **P4** is formed, various production channels are open. As shown in Figure 13, four channels from **P4**, denoted a–d, were found along the initial C–C activation branch, and each of them involves isomerization of **P4** with an H-migration transition state. Channels a and b both involve CH_4 elimination, and c and d involve loss of C_2H_4 and C_2H_6, respectively.

The energetically most favorable reaction path a produces methane and Sc^+ ethylene complex and is exothermic by

  0947-6539/03/0902-0495 $ 20.00+.50/0

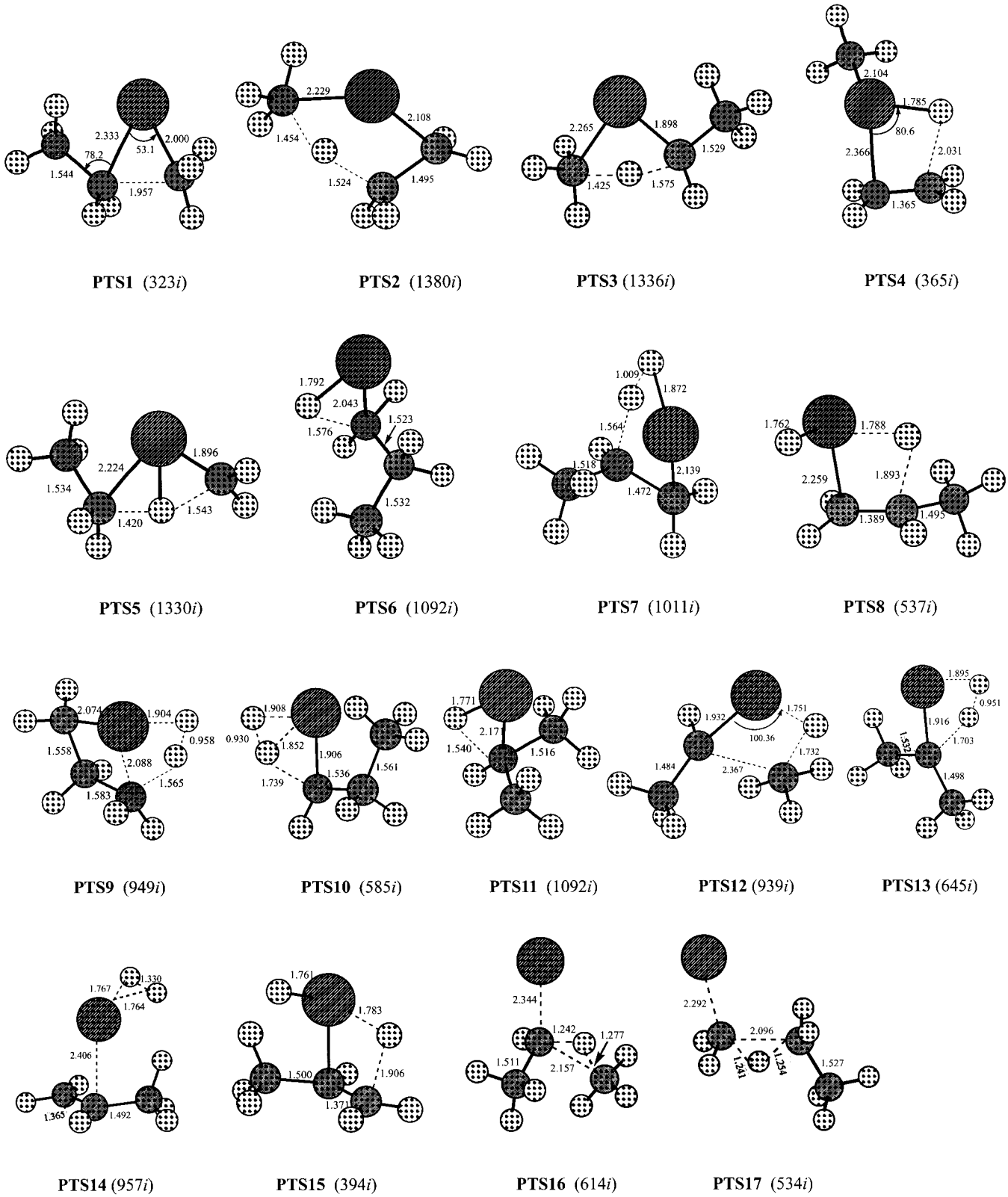

PTS1 (323*i*) **PTS2** (1380*i*) **PTS3** (1336*i*) **PTS4** (365*i*)

PTS5 (1330*i*) **PTS6** (1092*i*) **PTS7** (1011*i*) **PTS8** (537*i*)

PTS9 (949*i*) **PTS10** (585*i*) **PTS11** (1092*i*) **PTS12** (939*i*) **PTS13** (645*i*)

PTS14 (957*i*) **PTS15** (394*i*) **PTS16** (614*i*) **PTS17** (534*i*)

Figure 12. Optimized geometries [Å, °] of the first-order saddle points on the PES of [Sc, C_3, H_8]$^+$ at the B3LYP/6–311++G(d,p) level. The values in parentheses are the imaginary frequencies corresponding to the transition vectors.

20.4 kcal mol^{-1}. The channel involves the five-membered-ring transition state **PTS2**, in which an H atom is migrating from the terminal ethyl C atom to the methyl C atom to form the productlike intermediate **P5**, which is a complex of $Sc^+(C_2H_4)$ with methane. The calculated barrier height from **P4** to **PTS2** is 26.4 kcal mol^{-1}, 2.8 kcal mol^{-1} lower than the first step of the channel, C–C bond activation. Channel b is similar to channel a, but the H atom migrating to the methyl C atom

0947-6539/03/0902-0496 $ 20.00+.50/0 *Chem. Eur. J.* **2003**, *9*, No. 2

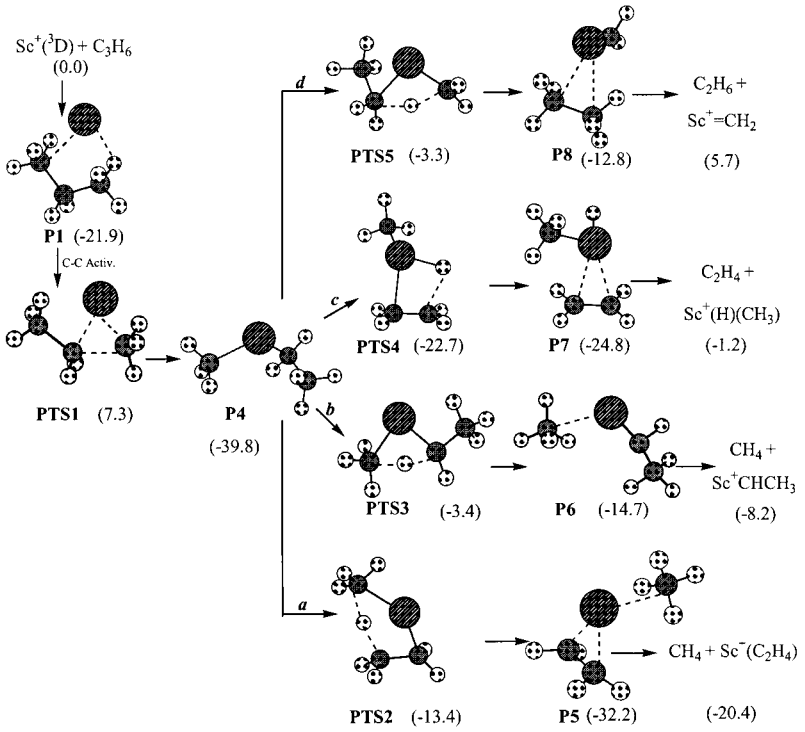

Figure 13. Reaction process following initial C–C activation on the PES of [Sc, C_3, H_8]$^+$.

comes from the methylene rather than the terminal methyl group. This process involves the four-membered-ring transition state **PTS3**, which connects intermediates **P4** and **P6**, a scandium ethyl carbene cation. The barrier height for this process is 36.4 kcal mol^{-1}, higher by 10.0 kcal mol^{-1} than the corresponding isomerization process in channel a. Channel c also involves a four-membered-ring transition state, namely, **PTS4**, in which a C–H bond of the methyl group is breaking and the Sc–H bond is forming. Following the path in both directions shows that this TS connects intermediates **P4** and **P7**, a complex of the methyl hydride of cationic scandium with ethylene. In the earlier studies by Holthausen and Koch[15] and Yi et al.[60], intermediates similar to **P7** were not found in the reactions of several late transition-metal ions, such as Fe^+ and Ni^+, with propane. Evidently the early and late transition-metal ions follow qualitatively different paths in their reactions with propane. The barrier height from **P4** to **PTS4** is 17.1 kcal mol^{-1}, 12.1 kcal mol^{-1} lower than that of C–C bond activation. Channel d produces ethane and scandium carbene cation. The transition state **PTS5** involved in this process resembles **PTS3**. In both cases, an H atom is migrating between two β-C atoms, but the origins of migration are different. In the second channel the H atom migrates from the methylene to the methyl group, while in the fourth channel the migrating H atom comes from the methyl group. The activation energies in the two processes are almost equal.

The energetic profile along the C–C bond activation branch is shown in Figure 14. The energetic bottleneck along this activation branch is the initial C–C bond activation.

Reaction pathway following initial primary C–H bond activation: The reaction process along the initial primary C–H bond activation branch is shown in Figure 15, and the corresponding energetic profile in Figure 16. The precursor in which Sc^+ will insert into the primary C–H bond is intermediate **P2**, which is slightly more stable by 0.4 kcal mol^{-1} than **P1**, the precursor of C–C bond activation. A TS structure of the primary C–H bond activation, namely, **PTS6**, was identified as a first-order saddle point connecting **P2** and **P9**, a C–H inserted species. We attempted to optimize the structures of the triplet and singlet staes of this TS, but only the singlet TS structure was located after a careful search. In the ground state of **PTS6**, the breaking C–H bond is elongated to 1.576 Å. The barrier height of primary C–H bond activation is 21.0 kcal mol^{-1}, 8.2 kcal mol^{-1} lower than that of C–C bond activation. Four product channels e–h from **P9** were found. As shown in Figure 14 they are four dehydrogenation reactions. Channel e is a 1,2-H_2 elimination reaction, which involves the five-membered-ring TS **PTS7**, in which a C–H bond of the methylene group is breaking and the H–H bond is forming. The structure of this TS resembles that of the productlike intermediate **P10**, a complex of cationic scandium–propylene with H_2. So **PTS7** is a late saddle point on the PES along the primary C–H activation path. The barrier height from **P9** to **PTS7** is 16.3 kcal mol^{-1}, lower by 4.7 kcal mol^{-1} than that of primary C–H bond activation. Channel f involves the dihydrido intermediate **P11**, which is a complex of the dihydrido Sc^+ species with propylene. The geometry of the intermediate is very similar to **E5** found in the reaction of Sc^+ with C_2H_6. However, the corresponding dihydrido minima $M^+(H)_2C_3H_6$ for Fe^+[15] and Ni^+[60] can not be located on the PES of [M, C_3, H_8]$^+$, and this case is similar to **P7**, that is,

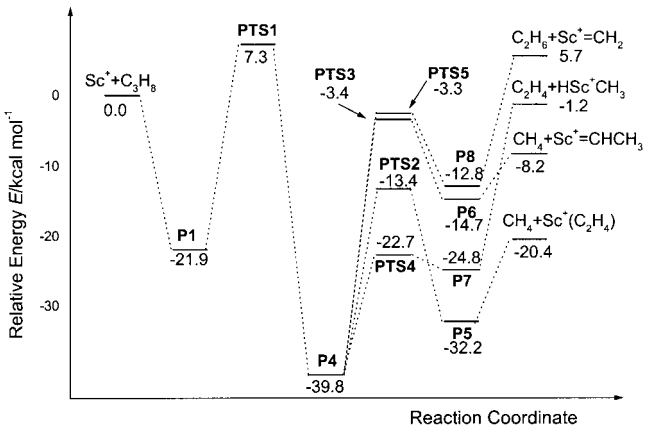

Figure 14. Energetic profile along the initial C–C bond activation branch in the reaction of Sc^+ with propane.

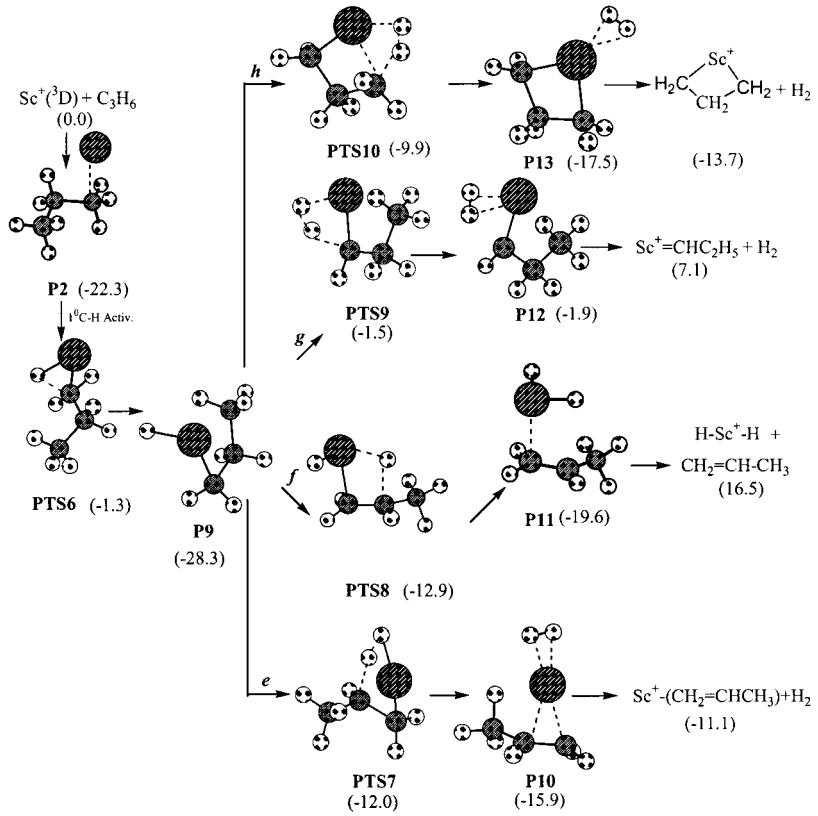

Figure 15. Reaction process following initial primary C–H activation on the PES of $[Sc, C_3, H_8]^+$.

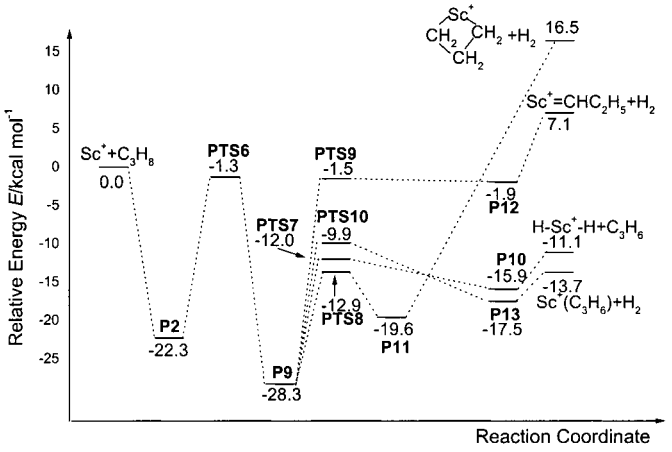

Figure 16. Energetic profile along the initial primary C–H activation branch in the reaction of Sc^+ with propane.

$M^+(H)(CH_3)(C_2H_4)$. Intermediates **P9** and **P11** are connected by **PTS8**, a four-membered-ring TS. The barrier height from **P9** to **PTS8** is 15.4 kcal mol^{-1}, slightly higher than that from **P9** to **PTS7**. The structure of **P11** apparently differs from that of **P10** (see Figure 11). In **P11** two H atoms form covalent bonds with cationic scandium, while in **P10** the corresponding two H atoms have almost formed molecular hydrogen. Intermediate **P11** exits by direct dissociation into the products $Sc^+(H)_2$ and CH_2=$CHCH_3$. The third and fourth possible channels from intermediate **P9** (g and h) are 1,1-H_2 and 1,3-H_2 elimination channels via **PTS9** and **PTS10**, respectively. Both TSs have four-membered-ring structures, and their forward products are **P12** and **P13**, respectively, two productlike intermediates. The barrier heights of the two processes are 26.8 and 18.4 kcal mol^{-1}, respectively.

Figure 16 shows that the saddle point **PTS6** corresponding to the initial primary C–H bond activation is the energetic bottleneck. This case is similar to the C–C activation branch.

Reaction pathway following initial secondary C–H activation: The initial complex of the secondary C–H activation branch on the PES of $[Sc, C_3, H_8]^+$ is **P3**, which is the most stable of the three ion–molecule complexes of Sc^+ and C_3H_8 found in this work. This complex has C_s symmetry and is calculated to be 0.8 and 0.4 kcal mol^{-1} stable than **P1** and **P2**, the initial complexes of C–C and primary C–H activation, respectively. Along the secondary C–H bond activation branch, this initial ion–molecule complex can be inverted to the C–H bond inserted species **P14**. This process involves the secondary C–H insertion TS **PTS11**. Similar to primary C–H activation, only a singlet TS structure corresponding to secondary C–H bond activation is located on the PES of $[Sc, C_3, H_8]^+$. In this TS, the breaking C–H bond is elongated to 1.540 Å. The imaginary frequency of the saddle point is 1092*i* cm^{-1}, and vibration analysis indicates that the transition vector mainly corresponds to breaking of the second C–H bond and formation of the Sc–H bond. The barrier height from **P3** to **PTS11** is 17.6 kcal mol^{-1}, lower by 3.4 kcal mol^{-1} than that of primary C–H bond activation. Along the reaction coordinate, the insertion intermediate **P14** can rearrange into four isomers, **P6**, **P15**, **P16**, and **P17** via four channels i–l, respectively. The isomerization of **P14** to **P6** along the channel i is connected by the four-membered-ring TS **PTS12**, in which C–C and Sc–H bonds are breaking and a C–H bond is forming. The direct dissociation of **P6** leads to $CH_4 + Sc^+$=$CHCH_3$. This is an alternative pathway for CH_4 elimination to the initial C–C activation branch (see Figure 14). However, the activation barrier of this process is as high as 58.6 kcal mol^{-1}, much higher than that of the two CH_4 elimination routes along the initial C–C activation branch. Two further isomerizations from **P14** are channels j and k, to form intermediates **P15** and **P16** via **PTS13** and **PTS14**, respectively. These processes are quite similar: channel j involves 2,2-H_2 elimination, and channel k 1,2-H_2 elimination. The activation energy is 26.0 kcal mol^{-1} for the former, and 25.1 kcal mol^{-1} for the latter. The last channel from **P14** (channel l) involves the dihydrido

0947-6539/03/0902-0498 $ 20.00+.50/0 *Chem. Eur. J.* **2003**, *9*, No. 2

minimum **P17**, in which the HSc^+H unit binds to propylene electrostatically. Structures **P14** and **P17** are connected by the saddle point **PTS15**. The barrier from **P14** to **PTS15** is 15.2 kcal mol^{-1}, that is, the lowest activation barrier among the four isomerization reactions from **P14**. The exit channel of **P17** is its simple dissociation to form $Sc^+(H)_2 + CH_2{=}CH{-}CH_3$.

The reaction process following secondary C–H bond activation is shown in Figure 17, and the energetic profile in Figure 18. Figure 18 shows that the energetically most favorable reaction channel is $Sc^+(^3D) + C_3H_8 \rightarrow$ **P3** $\rightarrow$ **PTS11** $\rightarrow$ **P14** $\rightarrow$ **PTS15** $\rightarrow$ **P17** $\rightarrow Sc^+(H)_2 + C_3H_6$. In this channel, the initial secondary C–H bond activation is the energetic bottleneck.

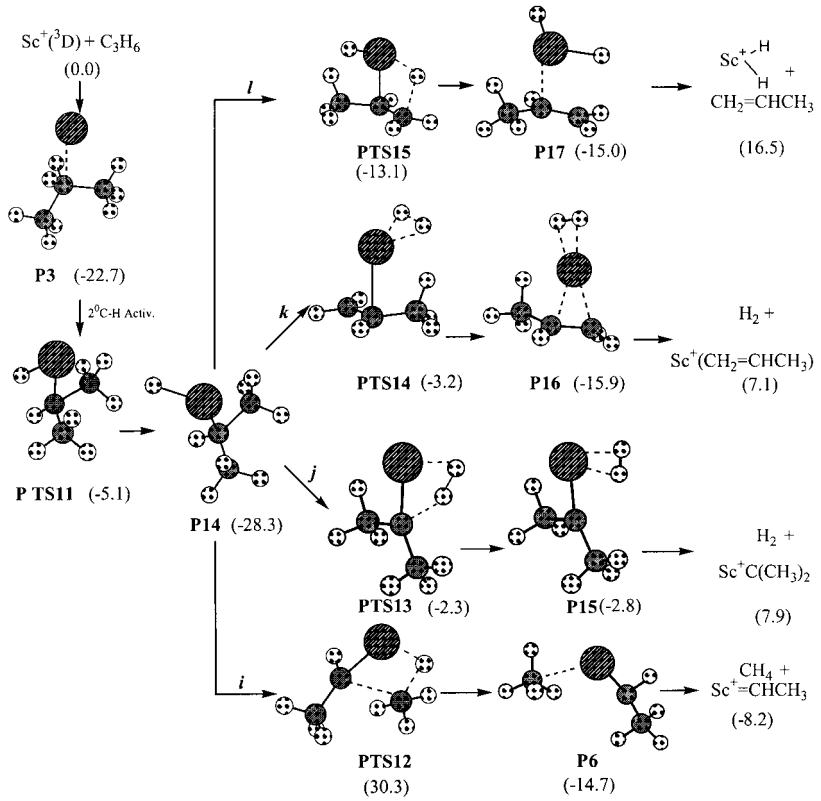

Figure 17. Reaction process following initial secondary C–H activation on the PES of $[Sc, C_3, H_8]^+$.

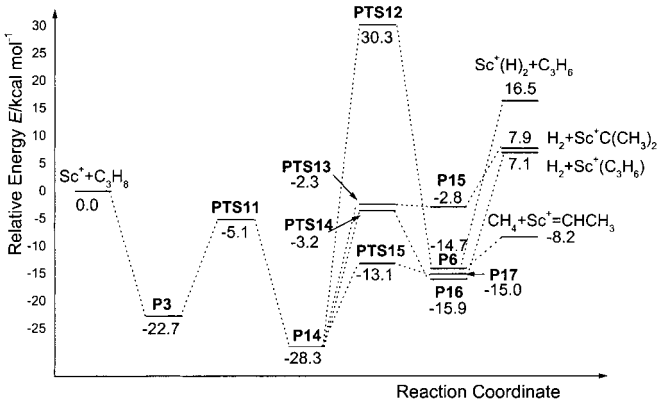

Figure 18. Energetic profile along the initial secondary C–H activation branch in the reaction of Sc^+ with propane.

Reaction pathway following synchronous C–H and C–C activation: On the PES of $[Sc, C_3, H_8]^+$ we find that, like $Sc^+ + C_2H_6$, the C–H and C–C bonds in propane can be also activated by Sc^+ synchronously while the two reactants approach one another. The concerted mechanism differs from the general consecutive mechanism of C–C and C–H activation, and could be a common channel for the reactions of transition-metal ions with alkanes. Two concerted channels were located along this branch. One is from **P3** to **P6** via saddle point **PTS16**, in which attack of Sc^+ on a methyl carbon atom of propane leads to C–C cleavage, and at the same time the methyl leaving group abstracts a hydrogen atom from the ethyl group. From the geometry of **PTS16** (Figure 12), it is clear that the C–C bond is breaking and an H atom is migrating from the methyl to the methylene group with a barrier of 55.7 kcal mol^{-1}. The other channel is from **P2** to **P8** via transition state **PTS17** with a barrier of 59.9 kcal mol^{-1}. In **PTS17**, Sc^+ attacks the methyl carbon atom of propane, and at the same time the ethyl leaving group abstracts a hydrogen atom from the methyl group. The geometry of **PTS17** is striking similar to that of **PTS16**. Our calculations show that the ground states of both **PTS16** and **PTS17** are triplets, so we conclude crossing between the triplet and singlet PESs occurs after the saddle points. Intermediates **P6** and **P8** are respectively precursors for direct loss of CH_4 and C_2H_6. Both these channels for synchronous C–C and C–H activation by Sc^+ require much higher activation energies than the successive activation of the C–H and C–C bonds on the PES and are unfavorable under low-energy conditions. However, the concerted reaction channels could be alternative pathways for the C–C and C–H activation of propane at higher energy. The reaction process and energetic profile are shown in Figures 19 and 20, respectively.

In summary, the reaction of Sc^+ with C_3H_8 is very similar to that of Sc^+ with C_2H_6, and involves two types of mechanisms: consecutive activation of C–C and C–H bonds (addition–elimination mechanism) and the concerted activation of C–C and C–H bonds. The former can process along three branches: C–C activation, primary C–H activation, and secondary C–H activation, each of which consists of two elementary steps: initial C–C or C–H activation of propane by Sc^+ to form inserted intermediates, and their subsequent isomerization. In these channels, which are energetically favorable at low energy, the initial C–C and C–H bond

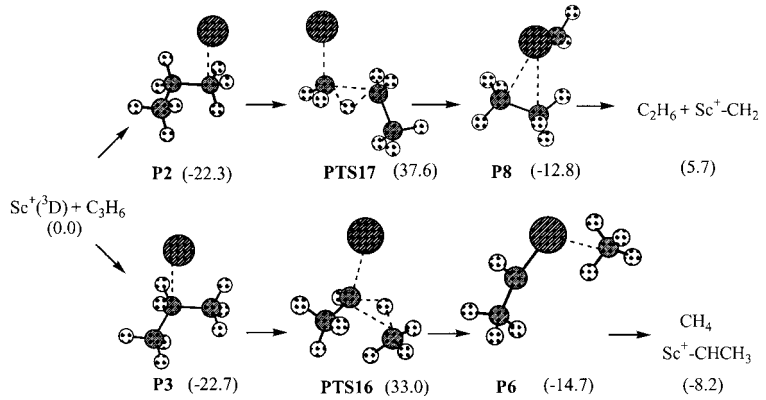

Figure 19. Reaction process following synchronous C–C and C–H activation on the PES of $[Sc, C_3, H_8]^+$.

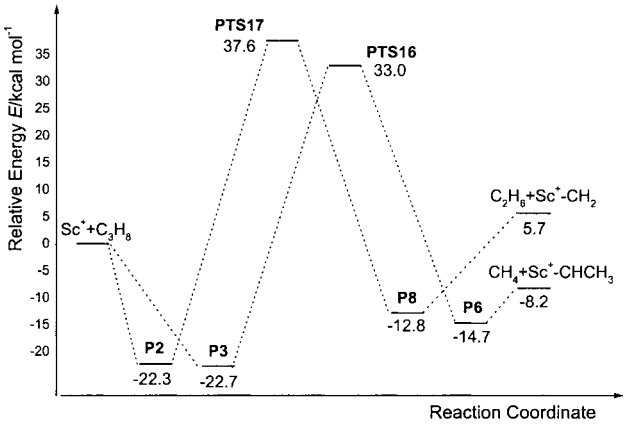

Figure 20. Energetic profile along the synchronous C–H and C–C activation branch in the reaction of Sc^+ with propane.

activations are generally the energetic bottlenecks. The latter involves an elementary step with a much higher activation barrier than the former. Although the concerted path is less favorable at low energy, it could be an alternative channel for the loss of small molecules such as CH_4 and C_2H_6 from $Sc^+ + C_3H_6$.

Conclusion

The gas-phase reactions of Sc^+ with CH_4, C_2H_6, and C_3H_8 have been systemically studied by using density functional theory. Our calculations provide further insight into the elementary steps of the mechanisms of C–C and C–H activations. The B3LYP/6-311++G(3df,3pd)//B3LYP/6-311++G(d,p) level of theory used here seems to be capable of describing the quantitative properties of the PESs of $[Sc, C_n, H_{2n+2}]^+$ ($n = 1-3$). The experimental bond dissociation energies of several species involved in the reactions of Sc^+ with C_nH_{2n+2} ($n = 1-3$) were reproduced. The errors introduced by calculations for the relative energies for different isomers are estimated to be ± 5 kcal mol^{-1}. Most of the reaction mechanisms proposed earlier on the basis of experimental findings have been confirmed. Moreover, we also found some new mechanisms for Sc^+-mediated C–C and C–H activations. It seems reasonable that mechanisms similar to the reactions of Sc^+ with C_nH_{2n+2} ($n = 1-3$) could also apply to the reactions of Sc^+ with larger alkanes, and to the reactions of other first-row transition-metal ions with alkanes. Further studies on the reactions of late first-row transition-metal ions are planned.

The following are the main conclusions drawn from the present theoretical calculations:

1) The ground states of the reactants $Sc^+(^3D) + C_nH_{2n+2}$ ($n = 1-3$) are triplets, while the ground states of the intermediates for insertion of Sc^+ into C–C and C–H bonds are singlets for all three systems. Hence, formation of the inserted species are spin-forbidden. This indicates that PES crossing occurs in the course of Sc^+ insertion into C–C and C–H bonds, and that the interaction between Sc^+ and C_nH_{2n+2} ($n = 1-3$) is strong as they approach each other. All subsequent rearrangements proceed along the singlet surfaces.
2) Crossing between the singlet and triplet surfaces occur before the saddle point for C–H activation, and after the saddle points for C–C and synchronous C–C and C–H activation.
3) The reactions of Sc^+ with alkanes are multichannel processes which involve two types of mechanisms: the addition–elimination mechanism and the concerted mechanism. The former involves two consecutive elementary steps: oxidative addition of a C–C or C–H bond to the metal center to form inserted species and subsequent reductive elimination of small molecules such as H_2, CH_4, and C_2H_6 after various isomerizations. The concerted mechanisms for CH_4 and C_2H_6 elimination from the reactions of Sc^+ with C_2H_6 and C_3H_8 are alternative pathways to the general mechanism proposed earlier. However, the activation energies of the concerted processes are higher than those of the consecutive processes.
4) The loss of CH_4 and/or C_2H_6 from $Sc^+ + C_nH_{2n+2}$ ($n = 2$ and 3) can proceed along both the initial C–C activation branch and the C–H activation branch. The loss of H_2 from $Sc^+ + C_nH_{2n+2}$ ($n = 2, 3$) can proceed not only according to 1,2-H_2 and/or 1,3-H_2 elimination mechanisms, but also by a 1,1-H_2 elimination mechanism.
5) In the energetically favorable addition–elimination reaction channels, the energetic bottlenecks are generally the initial C–C or C–H bond activation rather than the isomerization of the inserted intermediates. The concerted reactions involve only one elementary step, which is available only at high energy.
6) The oxidative addition of the C–C or C–H bond to the metal center in the reactions of Sc^+ with all three alkanes occur via a three-membered-ring transition state. While reductive eliminations of small molecules proceed via multicenter transition states, in most cases these involve four- or five-membered-ring structures.
7) Based on the similar reactivity of Sc^+ with three small alkanes, the results presented here can serve as a template for the reactions of Sc^+ with larger alkanes, or of other transition-metal ions with alkanes. The minima and

0947-6539/03/0902-0500 $ 20.00+.50/0 *Chem. Eur. J.* **2003**, *9*, No. 2

transition state geometries obtained here could act as model structures for searching for analogues in other systems composed of transition-metal ions and an alkane.

Acknowledgement

This work was supported by the National Science Foundation of China (No.: 20133020) and the Youth Science Foundation of Shandong University.

[1] G. D. Byrd, R. C. Burnier, B. S. Freiser, *J. Am. Chem. Soc.* **1982**, *104*, 3565–3569.
[2] N. Aristov, P. B. Armentrout, *J. Am. Chem. Soc.* **1986**, *108*, 1806–1819.
[3] C. Schulze, H. Schwarz, D. A. Peake, M. L. Gross, *J. Am. Chem. Soc.* **1987**, *109*, 2368–2374.
[4] R. Tonkyn, M. Ronan, J. C. Weisshaar, *J. Phys. Chem.* **1988**, *92*, 92–102.
[5] R. H. Schultz, J. L. Elkind, P. B. Armentrout, *J. Am. Chem. Soc.* **1988**, *110*, 411–423.
[6] P. A. M. van Koppen, J. Brodbelt-Lustig, M. T. Bowers, D. V. Dearden, *J. Am. Chem. Soc.* **1991**, *113*, 2359–2369.
[7] P. A. M. van Koppen, M. T. Bowers, E. R. Fisher, P. B. Armentrout, *J. Am. Chem. Soc.* **1994**, *116*, 3780–3791.
[8] P. A. M. van Koppen, M. T. Bowers, C. L. Haynes, P. B. Armentrout, *J. Am. Chem. Soc.* **1998**, *120*, 5704–5712.
[9] R. Georgiadis, P. B. Armentrout, *J. Phys. Chem.* **1988**, *92*, 7067–7074.
[10] J. Allison, R. B. Freas, D. P. Ridge, *J. Am. Chem. Soc.* **1979**, *101*, 1332–1333.
[11] D. G. Musaev, K. Morokuma, *J. Chem. Phys.* **1994**, *101*, 10697–10707.
[12] D. G. Musaev, K. Morokuma, *J. Phys. Chem.* **1993**, *97*, 11435–11444.
[13] M. C. Holthausen, W. Koch, *J. Am. Chem. Soc.* **1996**, *118*, 9932–9940.
[14] M. C. Holthausen, A. Fiedler, H. Schwarrz, W. Koch, *J. Phys. Chem.* **1996**, *100*, 6236–6242.
[15] M. C. Holthausen, W. Koch, *Helv. Chim. Acta*, **1996**, *79*, 1939–1956.
[16] D. G. Musaev, K. Morokuma, *J. Phys. Chem.* **1996**, *100*, 11600–11609.
[17] R. G. Parr, W. Yang, *Density Functional Theory of Atoms and Molecules*, Oxford University Press, Oxford, **1989**.
[18] J. K. Labanowski, J. W. Andzelm, *Density Functional Methods in Chemistry*, Springer, Berlin, **1991**.
[19] T. Ziegler, *Chem. Rev.* **1991**, *91*, 651–667.
[20] H. Cheng, D. B. Reiser, P. M. Mathis, K. Baumert, S. W. Dean, Jr., *J. Phys. Chem.* **1996**, *100*, 9800–9806.
[21] C. Lee, W. Yang, R. G. Parr, *Phys. Rev. B* **1988**, *37*, 785–789.
[22] B. Miehlich, A. Savin, H. Stoll, H. Preuss, *Chem. Phys. Lett.* **1989**, *157*, 200–206.
[23] A. D. Becke, *J. Chem. Phys.* **1993**, *98*, 5648–5652.
[24] P. J. Stephenes, F. J. Devlin, *J. Phys. Chem.* **1994**, *98*, 11623–11627.
[25] W. Koch, M. C. Holthausen, *A Chemist's Guide to Density Functional Theory*, Wiley-VCH, Weinheim, **2000**.
[26] M. N. Glukhovtsev, R. D. Bach, C. J. Nagel, *J. Phys. Chem. A* **1997**, *101*, 316–323.
[27] C. B. Kellogg, K. K. Irikura, *J. Phys. Chem. A* **1999**, *103*, 1150–1159.
[28] K. B. Wiberg, J. W. Ochterski, *J. Comput. Chem.* **1997**, *18*, 108–114.
[29] B. J. Smith, L. Radom, *Chem. Phys. Lett.* **1994**, *231*, 345–351.
[30] S. A. Kafafi, M. Krauss, *Int. J. Quantum Chem.* **1999**, *75*, 289–299.
[31] M. Peschke, A. T. Blades, P. Kebarle, *J. Am. Chem. Soc.* **2000**, *122*, 10440–10449.
[32] M. Pavlov, P. E. Siegbahn, M. Sandstrom, *J. Phys. Chem. A* **1998**, *102*, 219–228.
[33] M. Peschke, A. T. Blades, P. Kebarle, *J. Am. Chem. Soc.* **2000**, *122*, 1492–1505.
[34] D. Stockigt, *Chem. Phys. Lett.* **1996**, *250*, 387–392.
[35] K. Fukui, *J. Phys. Chem.* **1970**, *74*, 4161–4163.
[36] M. J. Frisch, G. W. Trucks, H. B. Schlegel, G. E. Scuseria, M. A. Robb, J. R. Cheeseman, V. G. Zakrzewski, J. A. Montgomery, Jr., R. E. Stratmann, J. C. Burant, S. Dapprich, J. M. Millam, A. D. Daniels, K. N. Kudin, M. C. Strain, O. Farkas, J. Tomasi, V. Barone, M. Cossi, R. Cammi, B. Mennucci, C. Pomelli, C. Adamo, S. Clifford, J. Ochterski, G. A. Petersson, P. Y. Ayala, Q. Cui, K. Morokuma, D. K. Malick, A. D. Rabuck, K. Raghavachari, J. B. Foresman, J. Cioslowski, J. V. Ortiz, A. G. Baboul, B. B. Stefanov, G. Liu, A. Liashenko, P. Piskorz, I. Komaromi, R. Gomperts, R. L. Martin, D. J. Fox, T. Keith, M. A. Al-Laham, C. Y. Peng, A. Nanayakkara, M. Challacombe, P. M. W. Gill, B. Johnson, W. Chen, M. W. Wong, J. L. Andres, C. Gonzalez, M. Head-Gordon, E. S. Replogle, J. A. Pople, Gaussian 98, Gaussian, Inc., Pittsburgh PA, **1998**.
[37] C. E. Moore, *Atomic Energy Levels*, National Bureau of Standards, Washington, DC, **1949**.
[38] M. A. Tolbert, J. L. Beauchamp, *J. Am. Chem. Soc.* **1984**, *106*, 8117–8122.
[39] P. B. Armentrout, *Top. Organomet. Chem.* **1999**, *4*, 1–45.
[40] S. G. Lias, J. E. Bartmess, J. F. Liebman, J. L. Holmes, R. D. Levin, W. G. Mallard, *J. Phys. Chem. Ref. Data Suppl.* **1988**, *17*, 1.
[41] C. W. Bauschlicher, Jr., *Chem. Phys. Lett.* **1995**, *246*, 40–44.
[42] A. Fiedler, D. Schröder, H. Schwarz, B. L. Tjelta, P. B. Armentrout, *J. Am. Chem. Soc.* **1996**, *118*, 5047–5055.
[43] M. A. Tolbert, J. L. Beauchamp, *J. Am. Chem. Soc.* **1984**, *106*, 8117–8122.
[44] L. S. Sunderlin, P. B. Armentrout, *J. Am. Chem. Soc.* **1989**, *111*, 4251–4262.
[45] L. S. Sunderlin, P. B. Armentrout, *J. Phys. Chem.* **1988**, *92*, 1209–1219.
[46] N. Aristov, P. B. Armentrout, *J. Phys. Chem.* **1987**, *91*, 6178–6188.
[47] L. F., Halle, P. B. Armentrout, J. L. Beauchamp, *J. Am. Chem. Soc.* **1981**, *103*, 962–963.
[48] R. H. Schultz, J. L. Eikind, P. B. Armentrout, *J. Am. Chem. Soc.* **1988**, *110*, 411–423.
[49] L. F. Halle, P. B. Armentrout, J. L. Beauchamp, *Organometallics* **1982**, *1*, 963–968.
[50] P. B. Armentrout, J. L. Beauchamp, *J. Am. Chem. Soc.* **1981**, *103*, 784–791.
[51] C. L. Haynes, Y. M. Chen, P. B. Armentrout, *J. Phys. Chem.* **1995**, *99*, 9110–9117.
[52] C. L. Haynes, Y. M. Chen, P. B. Armentrout, *J. Phys. Chem.* **1996**, *100*, 111–119.
[53] J. E. Bushnell, P. R. Kemper, P. Maitre, M. T. Bowers, *J. Am. Chem. Soc.* **1994**, *116*, 9710–9718.
[54] C. W. Bauschicher, Jr., H. Partridge, S. R. Langhoff, *J. Phys. Chem.* **1992**, *96*, 2475–2479.
[55] L. Sunderlin, N. Aristov, P. B. Armentrout, *J. Am. Chem. Soc.* **1987**, *109*, 78–89.
[56] M. Rosi, C. W. Bauschlicher, Jr., S. R. Langhoff, H. Partridge, *J. Phys. Chem.* **1990**, *94*, 8656–8663.
[57] D. J. Zhang, C. B. Liu, H. Q. Hu, Y. J. Liu, *Chin. J. Chem.* **2002**, *20*, 220–226.
[58] F. M. Bichelhaupt, T. Ziegler, *Organometallics* **1995**, *14*, 2288–2296.
[59] R. J. Noll, S. S.Yi, J. C. Weisshaar, *J. Phys. Chem. A* **1998**, *102*, 386–394.
[60] S. S. Yi, M. R. A. Blomberg, P. E. M. Siegbahn, J. C. Weisshaar, *J. Phys. Chem.* **1998**, *102*, 395–411.

Received: March 15, 2002
Revised: August 6, 2002 [F3957]

  0947-6539/03/0902-0501 $ 20.00+.50/0